DEVELOPMENT OF A MAGNETOCALORIC PUMP FOR APPLICATIONS IN HEAT PIPES

by

Juan Esteban Cataño Montoya

A thesis submitted in partial fulfillment of the requirements for the degree of

MASTER OF SCIENCE

in

MECHANICAL ENGINEERING

UNIVERSITY OF PUERTO RICO

MAYAGÜEZ CAMPUS

2005

Approved by:

_____ _____
Date

G. P. Peterson, PhD
Member, Graduate Committee

_____ _____
Date

Nellore Venkataraman, PhD
Member, Graduate Committee

_____ _____
Date

Gustavo Gutierrez, PhD
President, Graduate Committee

_____ _____
Date

Pablo Cáceres-Valencia, PhD
Representative of Graduate Studies

_____ _____
Date

Paul Sundaram, PhD
Chairperson of the Department

Abstract

A device that can pump a fluid with no moving mechanical parts represents a very encouraging alternative since such device would be practically maintenance free. A magnetocaloric pump achieves this purpose by providing a pressure gradient of a ferrofluid placed inside a magnetic field while experiencing a temperature change. If the temperature change is produced by extracting heat out of an element that needs refrigeration, coupling this heat via a heat pipe with the magnetocaloric pump will result in a completely passive cooling system. For applications near ambient temperature the ferrofluid must have specific characteristics such as low Curie temperature, high pyromagnetic coefficient, high thermal conductivity and low viscosity. This work presents the detailed description of the synthesis of ferrofluids composed of Mn-Zn ferrite nanoparticles and the characterization of its magnetic and thermal properties. Different composition of Mn-Zn ferrites nanoparticles were produce and evaluated. The best ferrofluid was compared with commercially available magnetite ferrofluid in a magnetocaloric pump prototype. Results of saturation magnetization, pyromagnetic coefficient, Curie temperature, particle size, viscosity and pressure increment inside the magnetocaloric pump are presented.

Resumen

La posibilidad de bombear fluido con un dispositivo que no presente partes móviles representa una alternativa muy prometedora ya que el mantenimiento del dicho dispositivo seria prácticamente cero. La bomba magnetocalorica cumple dicha función al generar un incremento en la presión de un fluido magnético que se encuentra dentro de un campo magnético y el cual al mismo tiempo sufre un incremento de su temperatura. Si el incremento de temperatura se produce extrayendo calor de un elemento que necesita refrigeración y llevándolo a la bomba magnetocalorica mediante un tubo de calor lo que se consigue es un sistema de refrigeración completamente pasivo. En aplicaciones con temperaturas cercanas a la temperatura ambiente se necesita que el fluido magnético tenga ciertas características como baja temperatura de Curie, alto coeficiente piromagnético, alta conductividad térmica y baja viscosidad. Este trabajo presenta una descripción detallada de la síntesis de ferrofluidos acuosos compuestos por nanoparticulas de la ferrita de Mn-Zn y se evalúan sus propiedades magnéticas y térmicas. Varias composiciones de ferrita de Mn-Zn son producidas y evaluadas y el ferrofluido con las mejores propiedades es comparado con ferrofluido comercial de magnetita en evaluaciones de la bomba magnetocalórica. Resultados de la magnetización de saturación, coeficiente piromagnético, temperatura de Curie, tamaño de partícula, viscosidad y el incremento de la presión dentro de la bomba magnetocalórica son presentados

Dedication

To my mother Myriam and my brother Héctor for their support, for being my inspiration and my biggest treasure. I love you both.

Acknowledgments

I would like to thank my advisor Dr. Gustavo Gutierrez for his honest and sincere counseling and support throughout this research and my Master's studies in general. I also would like to thank the members of my committee Dr. G. P. "Bud" Peterson, Dr. Nellore Venkataraman and professors Dr. Oscar Perales and Dr. Carlos Rinaldi and their students for their help and disposition. I would like to thank the Mechanical Engineering Department of the University of Puerto Rico at Mayaguez for their academic support and NASA for their financial support. Finally I would like to thank my friends for their help and all the memories.

Contents

List of Figures

List of Tables

1 INTRODUCTION

1.1 Motivation

This research investigates an alternative way to increase the heat transport capacity of heat pipes operating below 100 °C by coupling them with a convective system running by a magnetocaloric pump to remove heat from the condenser section of the heat pipe. This set-up can reduce the effective length of the heat pipe keeping it operational for higher heat fluxes. The proposed cooling system is passive, with no moving mechanical parts and the only energy source required is the heat that needs to be extracted from the application. This characteristic makes it ideal for application where maintenance is restricted, like in space applications. Another motivating aspect of the research is the use of ferrofluids, fluids with suspended small particles in the order of 3-15 nm that experience magnetization under the influence of a magnetic field. These ferrofluids promise enhancement in heat transfer applications due mainly to their improved thermal conductivity compared to the thermal conductivity of the base fluid [1]. This characteristic makes nanofluids in general (fluids with any suspended nanoparticles that do not have to be magnetic) attractive to cool high heat fluxes, which is a challenging issue in the area of heat transfer.

1.1.1 Magnetocaloric pump and magnetocaloric effect

A magnetocaloric pump provides a simple way of pumping fluid using only heat transfer and a magnetic field. The working principle is simple: magnetic materials lose magnetization as their temperature increases, reaching a point where they can no longer maintain a spontaneous magnetization, this temperature is called the Curie temperature. Figure 1.1 shows a typical magnetization vs. temperature curve for a given material with the y axis is expressed as the ratio between the magnetization at any temperature (M) and the saturation magnetization at a temperature of 0 K, *M(T)/Ms(0K)*, and the x axis is the temperature normalized with the Curie temperature, *T(K)/Tc(K)* [2].

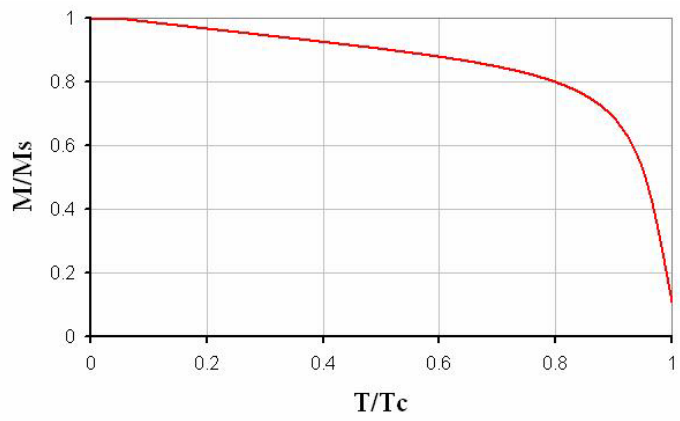

Figure 1.1 Domain magnetization as a function of temperature.

When a ferrofluid is inside a magnetic field coincident with a temperature gradient a pressure gradient is generated in the magnetic fluid [3]. As the fluid increases its temperature its magnetization decreases and it is displaced by the cooler fluid with higher magnetization (see Figure 1.2). The result is fluid propulsion with no moving mechanical parts.

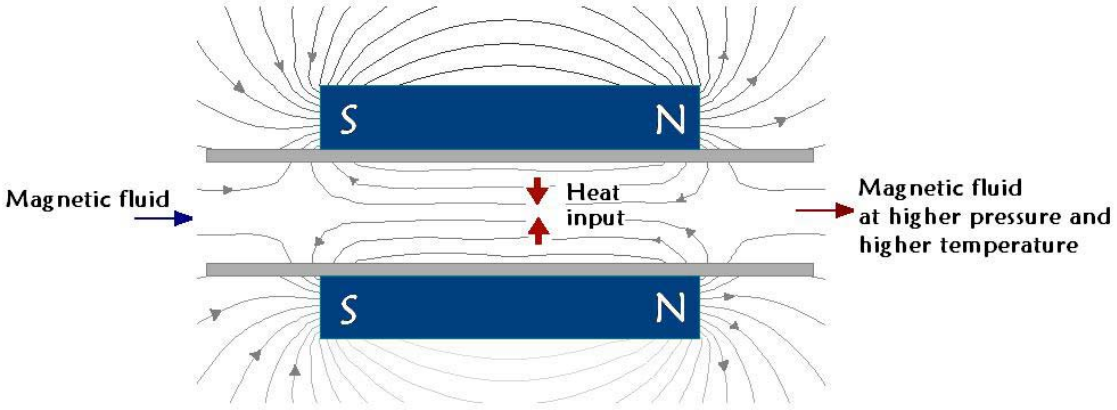

Figure 1.2 Schematic of a magnetocaloric pump

However, if the Curie temperature is far above the operational temperature of the system, the change in magnetization would be negligible. Most commercial grade magnetic fluids use magnetite nanoparticles and their Curie temperature is approximately 585 °C [2], too high for applications at operational temperatures near the ambient temperature at which many thermal systems work; so it is of great importance to the present investigation to obtain a ferrofluid with a Curie temperature near to 100 °C.

1.1.2 Heat pipes

A heat pipe is one of the most efficient devices to transport heat; among its advantages are its capacity to transport large quantities of heat through small cross-sectional areas over relative large distances, small end to end temperature drop and the possibility to transport and control high heat rates at different temperatures [4]. Figure 1.3 shows a schematic representation of a heat pipe. When heat is applied to one end of

the heat pipe (evaporation section), the working fluid vaporizes due to the higher temperature. The resulting pressure differential causes the vapor to travel to the other end of the heat pipe (condenser section), where a lower temperature causes the vapor to condense and give up its latent heat of vaporization. The condensed fluid is returned to the evaporator by capillary forces generated in an internal wick structure where the fluid is evaporated again (see Figure 1.3).

Usually, at the temperatures ranges of interest in this research, heat pipes are limited mostly by the capillary pressure generated at the porous of the wick structure. This capillary pressure has to overcome the hydraulic resistance in the wick; then the longer the heat pipe, the higher the pressure that needs to be overcome. If the capillary pressure is unable to overcome these loses then the evaporation section dries out and the heat pipe eventually fails [5]. A detailed literature review on the state-of-the-art of heat pipe technology can be found in Faghri [4], Peterson [5], and Silverstain [6].

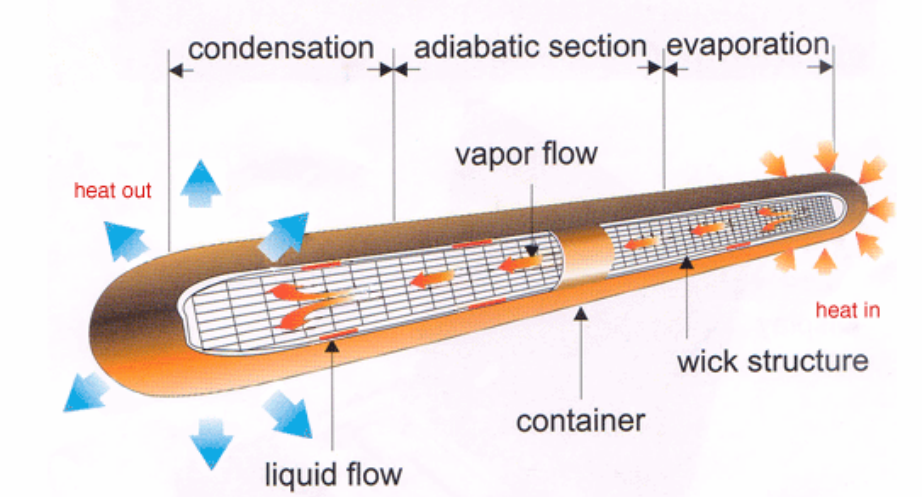

Figure 1.3 Schematic of Heat Pipe operation [7].

1.1.3 A Magnetic Heat Pipe Using the Magnetocaloric Effect

In this project a magnetocaloric pump is coupled with a heat pipe, to obtain a passive cooling system that has all the advantage of a heat pipe plus improving its capillary limit by reducing its effective length. The effective length of the heat pipe is reduced by coupling the magnetocaloric pump at a distance where the magnetic field is not prejudicial to any component of the application. The magnetocaloric pump removes the heat from the condenser section of the heat pipe and rejects it elsewhere by convection or radiation (see Figure 1.4). The maximum length of the magnetocaloric pump is determined by the pressure gradient produced in the ferrofluid to overcome the hydraulic losses inside the pump system.

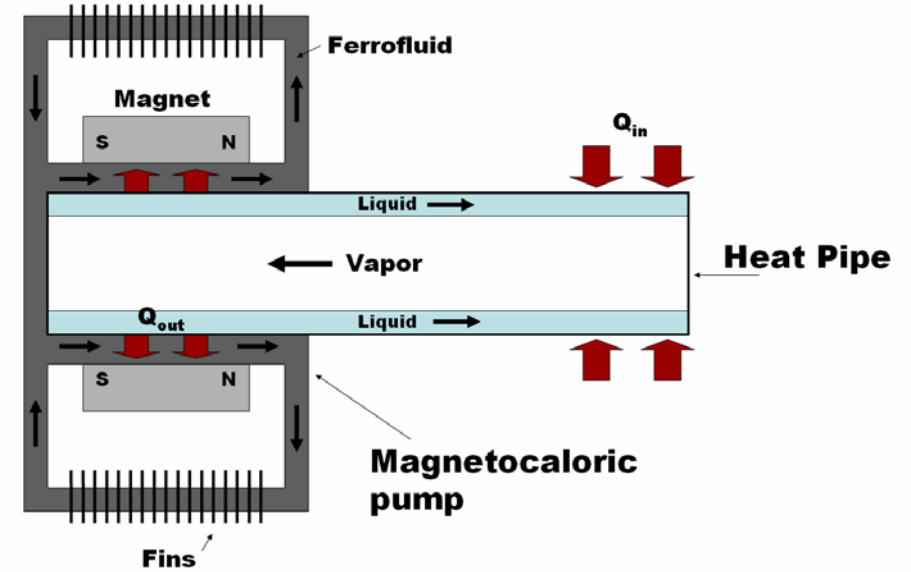

Figure 1.4 Representation of a passive magnetic cooling system.

1.2 Objectives

This research is focused on the study of magnetic mono-dispersed nanofluids exhibiting adequate magnetic and thermal properties for a passive refrigerating system composed of a magnetocaloric pump and a heat pipe.

The following aspects will be addressed:

a. Determination of the optimum composition of Mn-Zn ferrofluid by analyzing its magnetic and thermal properties.

b. Preparation of a stable magnetic nanofluid with suitable magnetic and thermal characteristics that enhances magneto-caloric energy conversion.

c. Construction and evaluation of the magnetocaloric pump with the synthesized ferrofluid.

2 REVIEW OF LITERATURE

This chapter presents some of the work done in the area of magnetocaloric energy conversion; magnetic fluid synthesis and magnetic characterization; thermal and rheological properties of nanofluids and other work that is relevant to the present research.

2.1 Magnetocaloric energy conversion

A magnetocaloric pump for microfluidic applications was proposed by Love et al. [8], using magnetic fluids with $Mn_{0.5}Zn_{0.5}Fe_2O_4$ nanoparticles suspended in water and in oil, with a Curie temperature of approximately 150°C and a magnetite ferrofluid suspended in oil. Experiments were carried out in such way that the only variable was the type of ferrofluid; keeping constant the heat input, the magnetic field and the temperature gradient inside the pump. In these experiments a 2-mm-diameter glass tube was used. The results showed a maximum velocity of 2.1 mm/s obtained for a temperature gradient (ΔT) of 13°C with a maximum temperature of 59°C for the water-based ferrofluid. The velocity of the fluid (V) was measured using a digital video camera and recording the displacement and time. Results were compared with calculated velocities using finite-element analysis (V_{FEA}). Table 2.1 shows a comparison for the different ferrofluids reported by Love et al. [8].

Ferrofluid	Spec. Grav.	Visc. (mPa-s)	Ms (kA/m)	T_{low} (°C)	T_{hi} (°C)	V (mm/s)	V_{FEA} (mm/s)
Magnetite in oil	1.4	375	27.85	74	86	0.17	0.23
$Mn_{0.5}Zn_{0.5}Fe_2O_4$ in oil	1.52	380	19.90	48	61	1.59	1.6
$Mn_{0.5}Zn_{0.5}Fe_2O_4$ in water	1.37	83	8.75	46	59	2.1	1.57

Table 2.1 Comparison of different ferrofluids in a magnetocaloric pump [8].

The results for the measured velocity (V) showed that the ferrofluid with $Mn_{0.5}Zn_{0.5}Fe_2O_4$ particles suspended in water has a velocity of more than an order of magnitude higher than that of the ferrofluid with magnetite particles in oil. This result makes the MnZn ferrite ferrofluid a good candidate for magnetocaloric energy conversion.

Shuchi, et al. [9], investigated experimentally the effect of position of the magnetic field on the heat transfer and driving force characteristics of a heat transport device using a binary mixture of a magnetic fluid and an organic solvent. This heat transport device uses the pressure difference due to magnetization losses as temperature increases in the fluid. The fluid consists of Mn-Zn ferrite nanoparticles dispersed in kerosene and n-hexane as the organic solvent with lower boiling temperature; the boiling saturation temperature of the binary magnetic fluid was measured as 356K, for a mass

concentration of n-hexane of 20%, and the decomposition temperature of the surfactant is 500K. A schematic of the testing section is presented in Figure 2.1; the experiments were done with a Reynolds number of 180 and a pipe diameter of 10 mm.

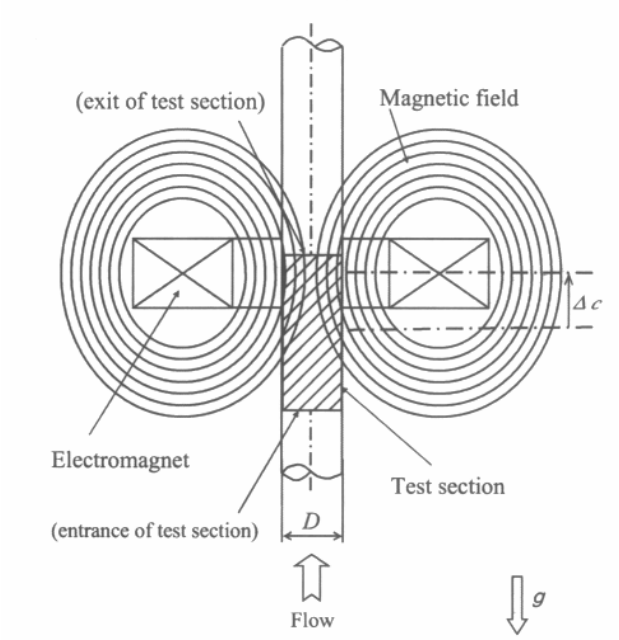

Figure 2.1 Representation of the test section [9].

Three magnetic field locations were tested and it was determined that the heat transfer and driving force increased when the magnetic field was placed closer to the entrance of the heating section while the worst case was when it was placed at the exit; in center position the pressure difference in the test section was increased only in lower magnetic field intensity and the Nusselt number did not change significantly.

Yamaguchi, et al. [10], designed and tested a device for converting heat to mechanical energy using a magnetic fluid that experiences a temperature change under

the influence of a magnetic field. The fluid is located between two pipes, one fixed and the other free for rotation. The fluid flow is generated by the pressure difference experienced in the fluid due to the change in magnetization as its temperature increases; a schematic of the working principle is presented in Figure 2.2. The rotary pipe should have moved by friction but the experiments did not achieve this result.

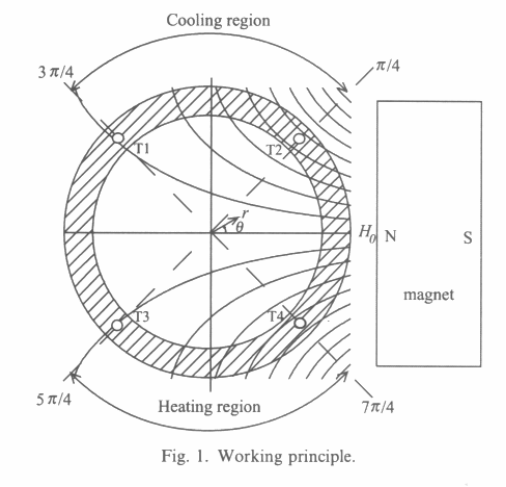

Fig. 1. Working principle.

Figure 2.2 Representation of a thermomagnetic driven motor [10].

To verify the numerical analysis temperatures of the experiments were compared with temperatures obtained from the numerical model at two different magnetic fields of 7960 A/m and 239000 A/m and a temperature difference of 10K. For both magnetic fields the results have the same trend but with significant difference at the lower magnetic field; however at high magnetic field results showed good agreement.

Another work by Yamaguchi, et al. include a numerical study of the flow

characteristics of a heat transport device that operates on a thermomagnetic cycle in which the magnetic pressure drives the fluid from a heat source to a heat sink; the device consists of two concentric pipes and a cylindrical magnet attached to the outer pipe, as shown in Figure 2.3 [11].

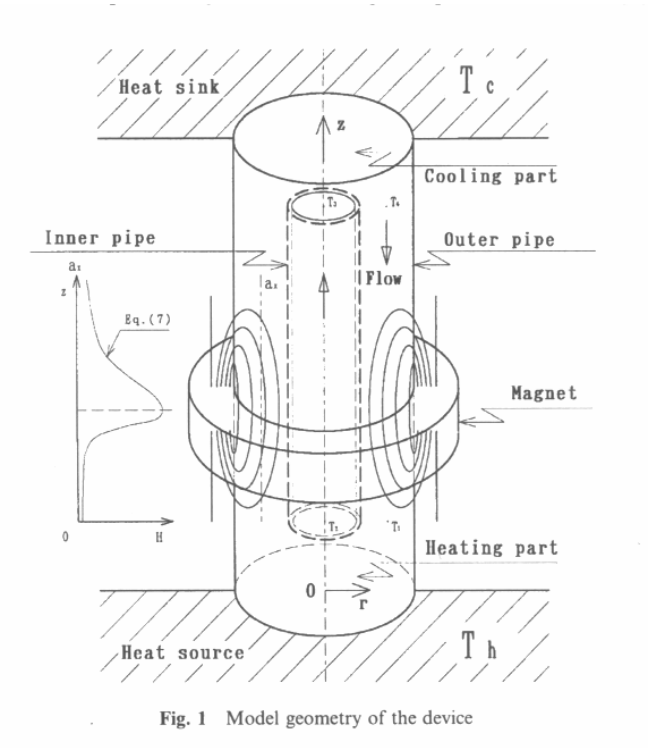

Figure 2.3 schematic of the heat transport device [11].

This work intended to find the optimum operating conditions for a heat transport device by controlling the magnetic field. Two cases were evaluated. Case 1: with the heat source in the lower end of the device and heat sink in the upper end. Case 2: just the opposite to Case 1, heating source on top and heat sink on the bottom of the device. Numerical results showed that the heat transfer may be increased or decreased by changing the strength of magnetic field. For the heating section on the bottom and low

Rayleigh numbers ($Ra < 10x10^3$), the heat transport capabilities increase as the magnetic field is increased while for higher Rayleigh numbers the Nusselt number tries to converge to the value of natural convection.

For Case 2 the values of Nusselt number are smaller and also the heat transport capabilities increase as the magnetic field is increased for small Rayleigh numbers; the Nusselt number tends to decrease as the Rayleigh number increases. These results indicate that high-performance of the device is only possible at moderate temperature differences when the magnetic field is increased.

Finally results for the Nusselt number for different conditions of temperature difference between hot and cold end and different magnetic fields are compared with previous experimental results but since the numerical simulations used different conditions that those in the experimental data, the model predictions could not be used to corroborate the actual behavior of the device. The experimental values showed a decrease in the heat transfer at the highest magnetic field and this is believed to be due to the change in viscosity of the magnetic fluid which is not taken into account in the numerical analysis.

Puri et al. [12], simulated numerically the heat transfer behavior of a magnetic fluid passing through a channel under the influence of an imposed magnetic field. The boundary conditions of the channel under investigation were adiabatic top wall,

isothermal bottom wall at 300K; a line dipole placed adjacent to the isothermal wall half way along the channel provides the external magnetic field (see Figure 2.4).

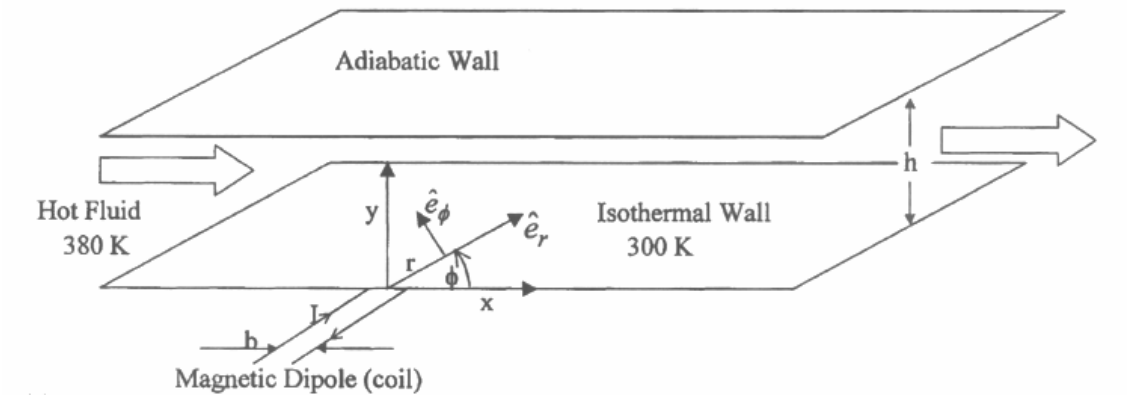

Figure 2.4 Flow configuration for numerical simulation [12].

A two-dimensional model showed that the heat transfer is enhanced as the external field strength increases; this was reflected in increasing values of the average Nusselt number. It was also appreciable that the flow was not influenced by low magnetic fields.

2.2 Magnetic fluid synthesis and magnetic characterization

Auzans et al. [13], presented the synthesis of Mn-Zn ferrite ferrofluids as well as its characterization. Two types of ferrofluids were synthesized: an aqueous cationic ferrofluid and a surfacted hydrocarbon-based ferrofluid. The Mn-Zn ferrite particles

($Mn_{1-x}Zn_xFe_2O_4$) were prepared by coprecipitation of aqueous solutions of $MnCl_2$, $ZnCl_2$ and $FeCl_3$ mixtures in an alkaline medium. Three different alkaline solutions were used: sodium hydroxide (NaOH), methylamine (CH_3NH_2) and ammonia (NH_3). It was found that for NaOH and CH_3NH_2, increasing the concentration of Zn in the ferrite leads to the formation of smaller particles. The nature of the coprecipitating base has also a significant influence on the size of the ferrite particle; the biggest size the ferrites were synthesized with NaOH while coprecipitation with NH_3 lead to the smallest particle size. For CH_3NH_2 and NH_3 formation of ferrite particles is limited to a specific range of Zn substitution: with $0 \leq x \leq 0.5$ and $0 \leq x \leq 0.2$ respectively. The maximum value of magnetization, at a field of 10.5KOe, was 49 emu/g for $Mn_{0.53}Zn_{0.47}Fe_2O_4$, further increase of Zn showed significant decrease in magnetization.

Zins, et al. [14], presented the synthesis and characterization of aqueous magnetic nickel-zinc ferrite fluids. The particles were prepared by coprecipitation of an aqueous mixture of metallic salts (nickel chloride $NiCl_2$, zinc chloride $ZnCl_2$ and iron(III) chloride $FeCl_3$) in alkaline medium (sodium hydroxide NaOH). The nanoparticles were prepared by pouring the metallic salts into the boiling alkaline solution; vigorous stirring and constant temperature were maintained for 90 minutes. The magnetic nanoparticles were first washed with distilled water and then dispersed in nitric acid (concentration of 2mol/L) during 15 minutes under vigorous stirring; this procedure creates positive surface charges but not enough to maintain the ferrofluid stable in time. The particles were mixed in a boiling solution of aqueous nitrate mixture ($Fe(NO_3)_3$, $Ni(NO_3)_2$ and

$Zn(NO_3)_2$) for 30 minutes; the resulting precipitate was washed with nitric acid (1mol/L) and then twice with acetone. The particles were finally dispersed in water (50 ml) and centrifuged and the supernatant was the finished ferrofluid. The magnetic characterization of the ferrofluid showed that the composition with the highest saturation magnetization (Ms) was $Ni_{0.66}Zn_{0.33}Fe_2O_4$ with a value of 70700 A/m.

Vekas, et al. [15], presented two preparation procedures: one for very concentrated magnetic fluids of magnetite nanoparticles on various polar liquids like propanol, butanol and decanol and the second one of low and medium concentrated magnetite particles on water. Magnetization curves for these ferrofluids were presented as well as comparisons between the propanol sample and low and medium concentration water-based samples for the low-field part of the magnetization curve. The first preparation procedure consisted of coprecipitation of Fe(II) and Fe(III) ions at 80°C, then a primary sterical stabilization with pure oleic acid at a temperature at least 80°C, decantation of the excess oleic acid, dispersion in a light hydrocarbon followed by a secondary stabilization with dodecylbenzensulphonic acid and finally a dispersion of the particles in the alcohol carrier. The second procedure for the water-based samples consisted of coprecipitation of Fe(II) and Fe(III) ions at 80°C, followed by washing and a double layer sterical stabilization with dodecylbenzensulphonic acid at 80°C; finally the particles were dispersed in water with sonication. The first procedure proved to be efficient in obtaining very concentrated magnetic fluid with saturation magnetizations between 650 and 920 G. Relative magnetization M/Ms curves of the most magnetic

samples are presented in Figure 2.5; where Ms is the saturation magnetization of the alcohol samples (C_3-C_{10}) and ϕ_p is the physical volume fraction of the magnetic particles. The alcohol magnetic fluids show excellent colloidal stability.

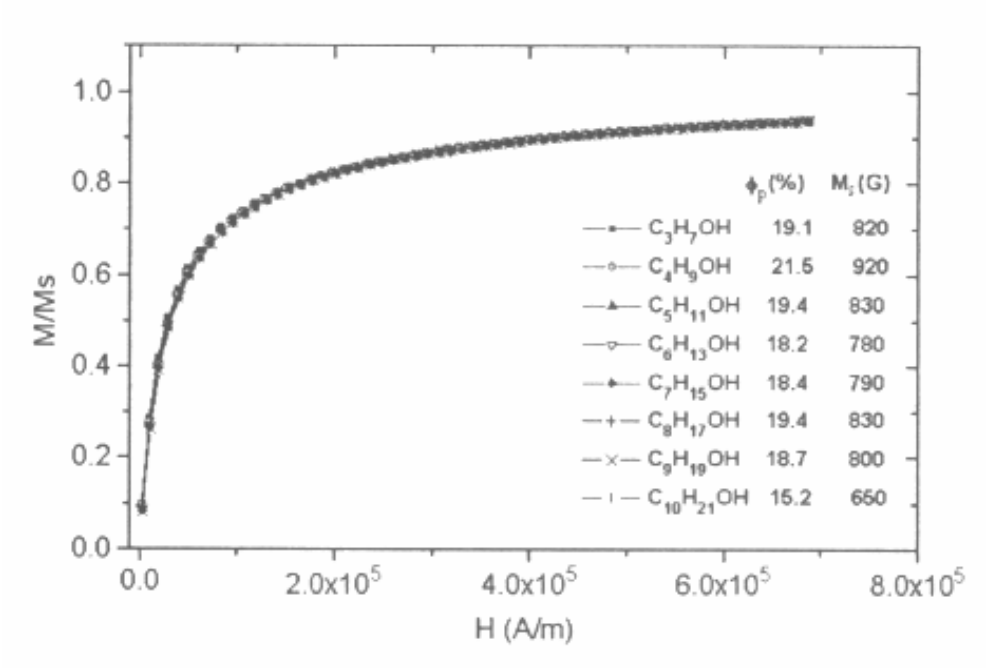

Figure 2.5 Magnetization curves of high concentration alcohol based magnetic fluids [15].

In Figure 2.6 two samples of water based ferrofluid, with volumetric concentrations of 9.3% and 2%, are compared with propanol based ferrofluid, which among the alcohol samples showed the highest initial susceptibility. The water-based ferrofluids have a maximum magnetization of about 400G but their stability decreases with increasing volume fraction of particles. The presence of agglomerates in the water-based samples is evidenced by their much greater initial susceptibility, compared to that of the propanol sample.

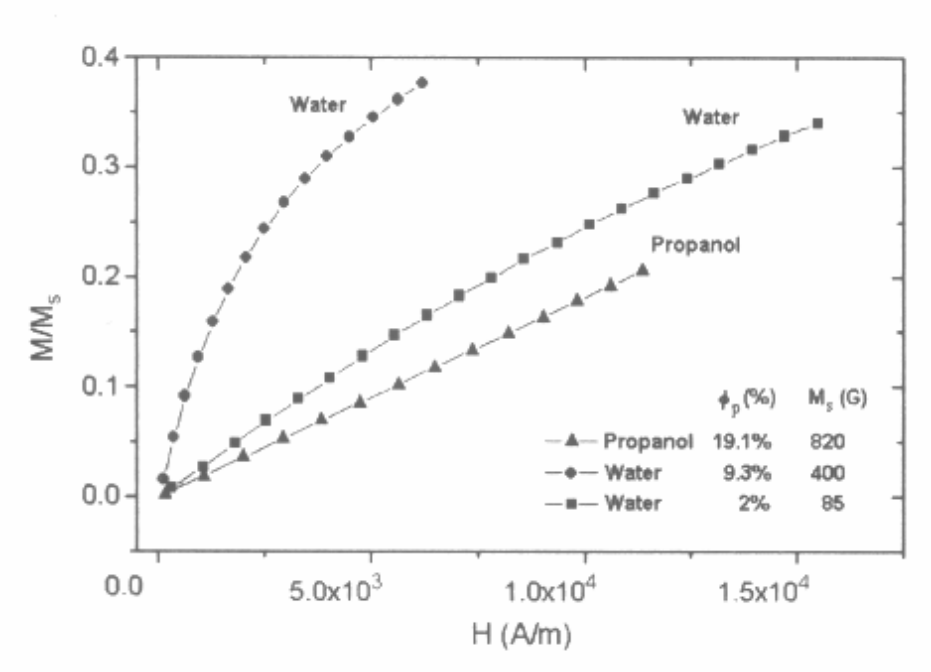

Figure 2.6 Low-field magnetization curves of propanol and water magnetic fluids [15].

Hatton, et al. [16], presented the use of two surfactants for the synthesis of water-based magnetic fluids of magnetite nanoparticles. Decanoic acid and n-alkanoic acids were used as the primary and secondary surfactants respectively (see Figure 2.7).

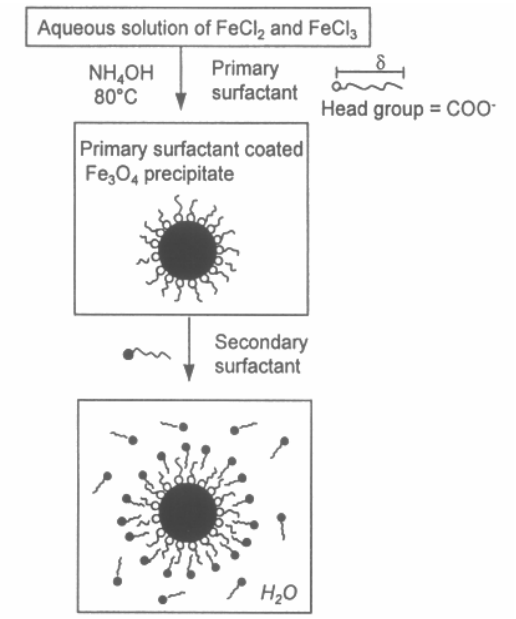

Figure 2.7 Representation of the synthesis of surfactant bylayer-stabilized magnetic fluid [16].

The researchers proposed that the surfactant bilayer can be divided into three zones: the innermost region composed of the primary surfactant, the outermost region composed of the second surfactant and the middle region composed of a combination of both surfactants. This technique allows stabilization of the nanoparticles as well as modification of their surface properties by changing the secondary surfactant as needed for a specific application.

Skumiel et al. [17], investigated the effect of particle concentration for a magnetite water based ferrofluid for three different samples with volumetric concentrations of 3.57 (sample 1), 1.785 (sample 2) and 0.893% (sample 3). The saturation magnetization of the samples, from the most concentrated to the lowest, are:

5529, 3591 and 2335 A/m. The magnetization curve is presented in Figure 2.8.

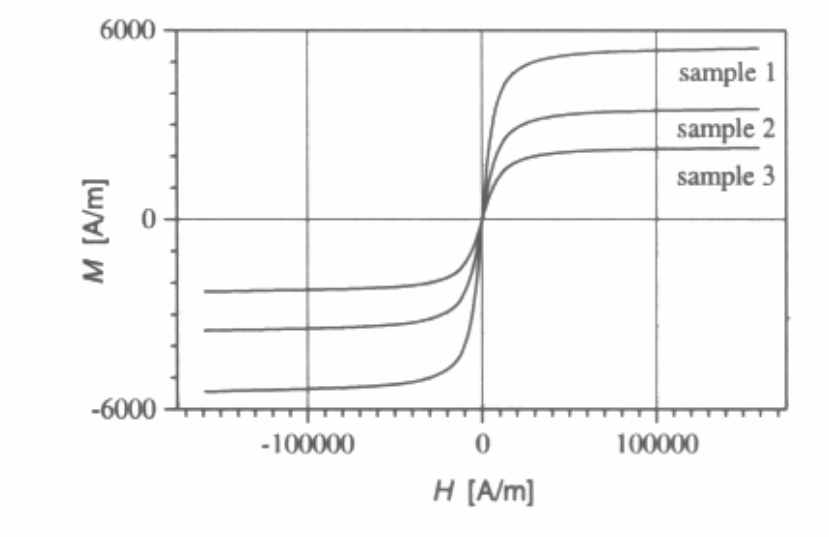

Figure 2.8 Magnetization curve for three samples with different concentrations: ϕ_1=3.56%, ϕ_2=1.785% and ϕ_3=0.893% [17].

The magnetization is not linearly dependant on the concentration of the magnetic particles; as it can be seen from Figure 2.8, which indicates the presence of interactions between particles and formation of clusters.

Maiorov et al. [18], studied the magnetic properties of $Mn_{0.5}Zn_{0.5}Fe_2O_4$ and the effect of particle size. Two fractions were separated by centrifugation from an initial ferrofluid of hydrocarbon based colloid with $Mn_{0.5}Zn_{0.5}Fe_2O_4$ stabilized by oleic acid. Mean particle diameters of the two samples, determine by TEM (Transmission Electron Microscope) measurements, are 6.2 nm and 9.7nm. Magnetic measurements were performed at a temperature range of 100-295K and no magnetic saturation was achieved

for a maximum magnetic field of 120000Oe. Figure 2.9 shows the magnetization curves for the original ferrofluid (initial colloid) and the two samples separated by centrifugation. The difference in magnetization for the three samples is attributed to a change in concentration due to the centrifugation process.

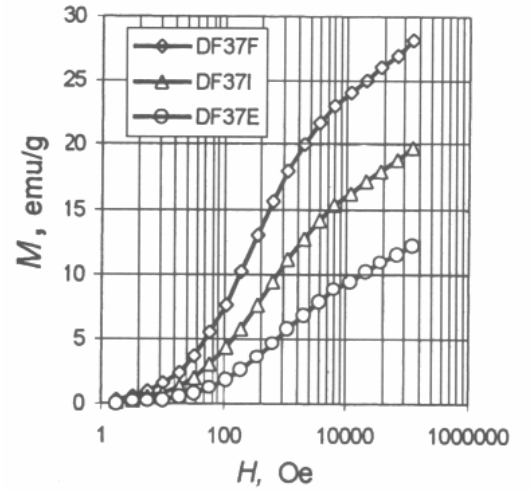

Figure 2.9 Magnetization curve for three ferrofluid samples with different particle size at 100K: DF37F=9.7nm, DF37E=6.2nm and DF37I=initial colloid [18].

It was also suggested by the researchers that the relative pyromagnetic coefficient $\frac{\partial M_s}{\partial T}\frac{1}{M_s}$ does not depend on the particle size; for both samples the saturation magnetization falls approximately in the same proportion when the temperature is increased from 100K to 295K (see Figure 2.10). The Curie temperature was not estimated because the temperature interval of the study was too small.

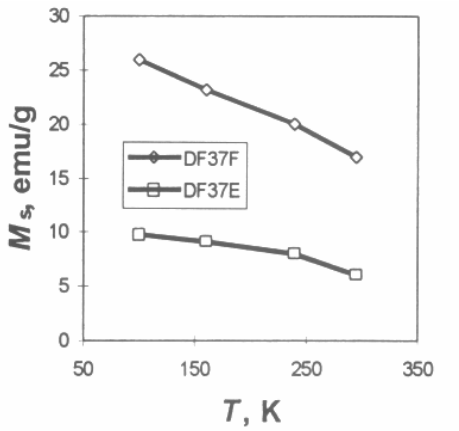

Figure 2.10 Dependance of magnetization on temperature for two different particle size: DF37F=9.7nm and DF37E=6.2nm [18].

Srikanth et al. [19], studied the role of surfactants and inter-particle interactions of Mn-Zn ferrite nanoparticles. Two different surfactants were used: bis-(2-ethylhexl) sodium sulfosuccinate, which is referred as AOT and a mix of nonylphenol poly(oxyethylene)$_5$ and nonylphenol poly(oxyethilene)$_9$, referred as NP. The stoichiometry of the samples was determined using ICP (Inductively Coupled Plasma) analysis and the results showed a slight loss of Zn for the AOT sample $Mn_{0.68}Zn_{0.25}Fe_{2.07}O_4$ while for the NP sample the stoichiometry analysis was $Mn_{0.65}Zn_{0.38}Fe_{1.98}O_4$. TEM studies showed that the average particle size was nearly 20 nm for both samples but analysis done with XRD (X-Ray Diffraction) suggested particle size for the AOT to be 14.6 nm and for the NP 10.8 nm; representing a considerable difference in particle size. The saturation magnetization at 300K of both samples was calculated as 44 emu/g for NP and 57 emu/g for AOT, which is consistent with previous values reported for Mn-Zn ferrites by Son et al. [20], in which $Mn_{0.5}Zn_{0.5}Fe_2O_4$ nanoparticles produced by plasma torch synthesis showed a saturation magnetization of

47.1 emu/g.

Sattar et al. [21], studied the effect of the non-magnetic Aluminum Al^{3+}-ion substitution on the magnetic properties of Mn-Ni-Zn ferrite. The effect of Al^{3+}-ion substitution was studied for the $Mn_{0.5}Ni_{0.1}Zn_{0.4}Al_xFe_{2-x}O_4$ ferrite with x varying from 0 to 0.15 with increments of 0.025. The saturation magnetization of the samples had a minimum of 21.03 emu/g for x=0 (no Al^{3+}-ion substitution) and a maximum magnetization of 24.68 emu/g for x=0.05; also the Curie temperature had a minimum at x=0 of about 430K and a maximum of 525K with x=0.05. Previous results from Amarendra et al. [22] and Rezlescu et al. [23] showed that Mn substitution on Ni-Zn ferrites enhanced its saturation magnetization and decreased the Curie temperature as the content of Mn increased.

Additional information description of the synthesis of aqueous nanofluids can be found at the Materials Research Science and Engineering Center (MRSEC) webpage [24]. Nanoparticle seeding-assisted synthesis and size selection procedures are described by Perales and Chinnasamy ([25];[26]).

2.3 Thermal and rheological properties of nanofluids.

Xuan and Li [27] proposed a model to describe heat transfer performance of nanofluids flowing inside a tube, also presented a theoretical study of the thermal

conductivity of nanofluids and using the hot-wire method measured the thermal conductivities of nanofluids with copper particles. Results showed an increase of 24% to 78% of the thermal conductivity of the nanofluid to that of the base fluid for volume fractions from 2.5% to 7.5% respectively. An expression for predicting Nusselt number was derived but no experimental data is presented to verify the correlation.

The influence of temperature in the behavior of magnetic fluid with $Mn_{0.6}Fe_{0.4}Fe_2O_4$ nanoparticles was analyzed by Caizer [28]. Magnetization curves for 300, 246 and 90K showed that hysteresis appears at the lowest temperature with a well emphasized loop. A saturation magnetization curve for temperatures from 90 to 300K was fitted using a variation of the $T^{3/2}$ law and the results showed good agreement and confirmed the increase of the mean magnetic diameter of the fluid (kerosene with $Mn_{0.6}Fe_{0.4}Fe_2O_4$ nanoparticles coated with oleic acid) when its temperature decreases.

Grulke et al. [29], studied the effect of carrier fluid type, nanoparticle concentration and nanoparticle source and relate the increase of thermal conductivity with the increase heat transfer coefficient. Two different types of oils were used as the carrier fluids for graphite nanoparticles with weight concentration of 2% and 2.5%. The following physical properties of the nanofluids were measured: thermal conductivity using the hot-wire method, density measured with a pycnometer, heat capacity measured with a differential scanning calorimeter and kinematic viscosity was measured using a reverse tube capillary viscometer. Results showed that thermal conductivity had a

maximum increase of 56% over the carrier fluid, for the most concentrated nanofluid. Density and heat capacity did not change much as compared to those of the carrier fluid. The nanoparticles increase the heat transfer coefficient of the fluid system in laminar flow but the increase was less than predicted by current correlations based on static thermal conductivity measurements.

Buioca et al. [30], proposed a method to obtain magnetic fluids with lower viscosity from an original sample and maintaining the same saturation magnetization. The lower viscosity of the ferrofluid was reached by decreasing the particle interactions and polidispersivity. Previous theoretical and experimental studies have shown the presence of solid phase with low magnetic properties in magnetic fluids; increasing the viscosity but not the magnetic properties of the ferrofluid. Also small cluster formation, in which smaller particles are attracted by the larger ones, increases significantly the viscosity of the magnetic fluid. A device for the separation of particles with low magnetic contribution and smaller size is presented in Figure 2.11.

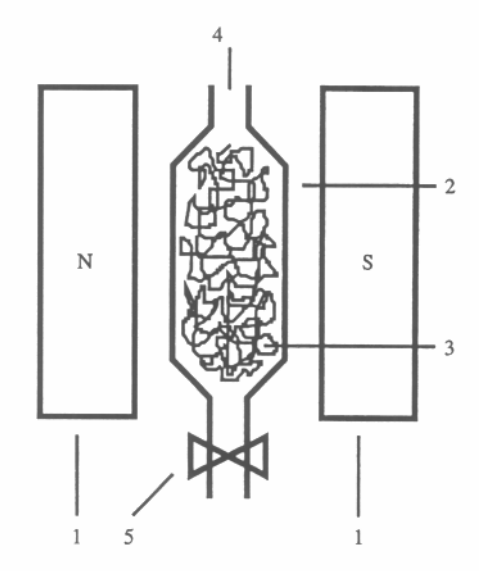

Figure 2.11 Schematic of the device for magnetic particle separation [30].

The device consists of an electromagnet (numbered as 1 in Figure 2.11) and a vertical glass tube, 2, with an open end at the top, 4, and a valve at the bottom, 5, that is filled with the ferrofluid, 3. By applying an adequate magnetic field and liquid flow through the glass tube the particles with higher magnetization are retained while the other particles are removed by the flow inside the tube. The fluid inserted in the glass tube is the same as the carrier of the ferrofluid. The final concentration of the samples varied but forced evaporation was used to obtain concentrations close to the original ferrofluid. Results showed that the viscosity for the sample with the narrower distribution of nanoparticles had a viscosity coefficient about two times lower than the original ferrofluid for the same saturation magnetization.

Wagh and Avashia [31], derived a formula for the viscosity of magnetic fluids in

terms of the ratio of solid particles per unit volume (n_2) and number of fluid molecules per unit volume (n_1) of the suspension, n_2/n_1, the ratio of the mass of each suspended particle (m_2) and molecular mass of the fluid (m_1), m_2/m_1, a relation between the size of the solid particles and the fluid molecules, and the magnetic field.

Schmidt [32] synthesized magnetic fluids with hybrid particles of magnetite (Fe_3O_4) and ε-Caprolactone that showed a thermal transition during induction heating which can be useful in medical applications such as controlled drug release.

2.4 Additional related work

Numerical simulations of magnetic fluids also include the research of the heat transfer behavior of ferrofluids in steady magnetic fields inside a rectangular cavity, carried out by Tangthieng, et al. [33], in which the finite element simulations showed significant enhancement in the heat transfer with an increment of 45% in the Nusselt number for a magnetic field of 562 G. This indicates that a nanofluid is a good alternative for cooling applications.

Ivanov and Mendelev [34] solved analytically the problem of equilibrium chain lengthening in magnetic fluids for the case of noninteracting chains. Their results showed the influence of the chain aggregates on the magnetostatic properties of the fluid and they also noticed that the chain interaction is important and should be taken them into account

for proper comparisons.

Ouakssim, et al. [35], used nuclear magnetic relaxation dispersion (NMRD) profiles and magnetometry (fitting the NMRD profiles by the appropriate theory) as control parameter for the reproducibility of magnetic fluids; this method allows the determination of the average radius and the specific magnetization.

Zabow et al. [36], presented the control of flow with microparticles inside microchannels by applying electric and magnetic fields to position the particles in the center of the microchannels, eliminating the adhesion to channel wall and particle settling among other characteristics. Odenbach [37], discussed thermomagnetic convection, in which a ferrofluid can be driven and controlled using magnetic forces.

2.5 Contribution of this research

From the results obtained by Love et al. [8] ferrofluid with suspended MnZn ferrite nanoparticles is selected for application in a magnetocaloric pump operating at low temperature. The present research investigates what composition of MnZn ferrite nanoparticles is best suited for the proposed application and a detailed characterization of its magnetic and thermal properties is presented including measurements of saturation magnetization and pyromagnetic coefficient; determination of particle size; estimation of Curie temperature of the ferrofluid; measurement of effective thermal conductivity of the

ferrofluid and viscosity for different concentrations of particles in the base fluid. The proposed magnetocaloric pump allows evaluation at different applied magnetic fields and for different temperature gradients; the magnetocaloric pump prototype allows easy change of the magnetic field section and the length and the strength of the magnetic field can be change and the heat applied is controlled by a variable transformer. Also the position of the heat source with respect of the magnetic field can be varied. This will allow corroborating the results presented by Shuchi et al. [9]. The ferrofluid synthesis is based on the work done by Perales, Chinnasamy and Auzans et al. ([26],[25],[13]) and the results are compared based on saturation magnetization and volumetric concentration of nanoparticles. This research contributes to the better understanding of magnetocaloric pumps and the parameters that are important in its operation which include properties for the ferrofluid that is used in the pump.

3 MAGNETIC FLUIDS

3.1 Introduction to Magnetic behavior of Materials

Magnetism exhibits an identifiable dipole orientation and no monopole has ever been discovered; so there are always two magnetic poles in a magnetic field separated by a finite distance. The dipole behavior extends down to magnetic dipoles in atoms, where many atoms have a permanent magnetic moment. The net magnetic moment of an assembly of atoms is generally zero, due to the random orientation of atomic moments within the assembly. The orbital motion of electrons around the nucleus and the spinning motion around their axes, within the atoms, produce the magnetic field associated with that atom. The small contribution from protons and neutrons is usually neglected.

When a magnetic field is applied, materials react in a certain way. According to their magnetic behavior, materials can be classified as: ferromagnetic, antiferromagnetic, ferrimagnetic, paramagnetic and diamagnetic.

Ferromagnetic materials include iron, cobalt and nickel and some rare earths, such as gadolinium. In this type of materials dipolar interaction promotes parallel alignment of the dipoles; resulting in a material that may have net magnetization in the absence of an external field (see Figure 3.1 (a)). Large magnetic fields can be retained or eliminated as

desired in ferromagnetic materials, giving them a great engineering importance.

Antiferromagnetic materials do not exhibit any net magnetization even in the presence of a magnetic field. In these materials the dipoles of adjacent atoms are aligned in opposite directions (Figure 3.1 (b)). Manganese and Chromium in solid state at room temperature exhibit antiferromagnetism.

In ferrimagnetic materials the dipoles of adjacent atoms align in opposite directions but the magnitude or the number of moments pointing in one direction is different than the ones pointing in the opposite direction; creating a considerable net magnetization in the absence of a magnetic field (Figure 3.1 (c)). In general ferrimagnetic materials have lower magnetization than ferromagnetic materials because of the effect of the opposed dipole moments. Magnetite (Fe_3O_4) and ferrites (MFe_2O_4) are examples of ferrimagnetic materials.

Paramagnetic behavior is exhibited by materials in which the atomic moments tend to align under the presence of a magnetic field (Figure 3.1 (d)), this magnetic effect is small and disappears when the magnetic field is removed. Some examples of paramagnetic materials are aluminum, platinum, calcium and sodium.

Diamagnetic materials behave similar to paramagnetic materials but the magnetic

moments of the atoms aligned opposite to the applied field, producing a very small negative magnetic effect; smaller in magnitude than the paramagnetic effect. Copper, silver and gold show diamagnetic behavior (see Figure 3.1 (d)).

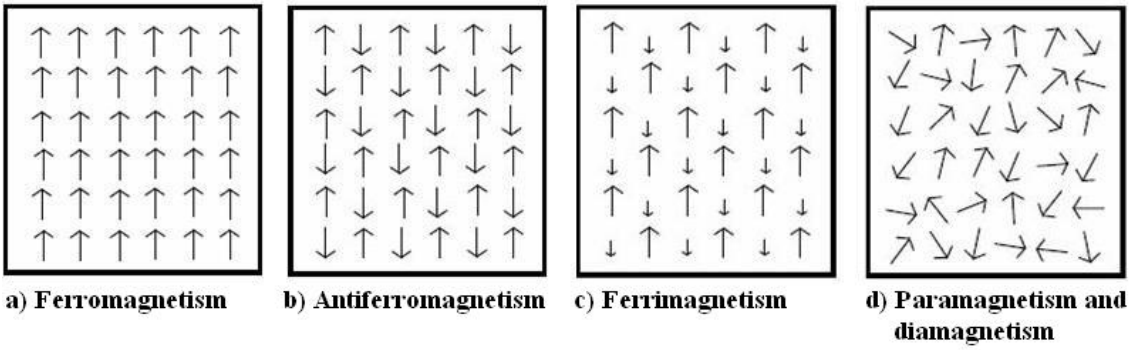

Figure 3.1 Orientation of magnetic moments for different types of magnetic behavior.

Typical magnetization curves for the different types of magnetic behavior are presented in Figure 3.2. Some important parameters shown are: saturation magnetization (M_s), is the maximum value of magnetization that a material can experience under the influence of any magnetic field, at this point all the dipoles are aligned in the direction of the external magnetic field; remanence magnetization (M_r), represents the capacity of a material to maintain its magnetic dipoles aligned after the magnetic field is removed (permanent magnet); coercivity (H_c), represents the magnetic field needed to demagnetize the material; magnetic susceptibility, χ, represents the strength of the response to an external magnetic field ($\frac{\partial M}{\partial H}$). Ferrimagnetic behavior is similar to ferromagnetic but it may differ in the values of M_s, M_r and H_c. Antiferromagnetic materials behave like

diamagnetic at low temperature, but can sometimes display ferromagnetic behavior.

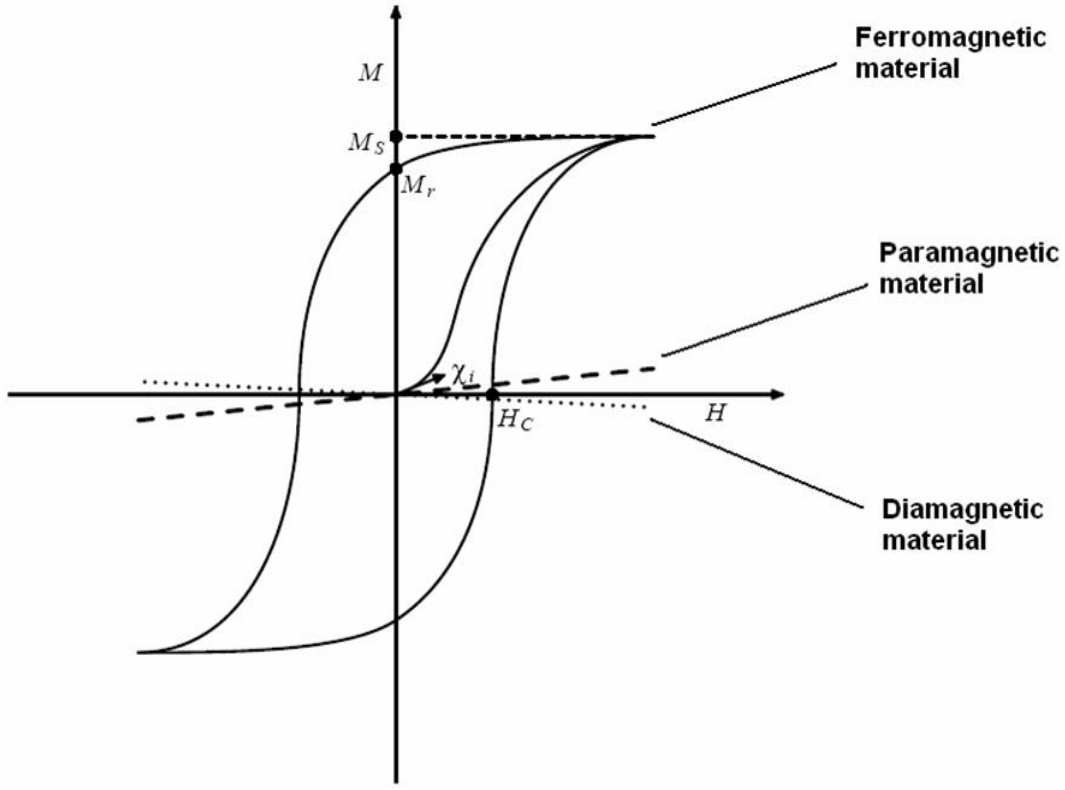

Figure 3.2 Magnetization curve for different types of materials.

3.2 Magnetic Domains

In a magnetic material there are small volume regions where the magnetic moments of neighboring atoms are oriented in a fixed direction spontaneously, this regions are called domains. Domains minimize the field energy in the material, which would be considerable if the material were magnetized in one direction; for a unit volume of a ferromagnetic material, a single domain structure has the highest potential energy (Figure 3.3*a*). By dividing the single domain into two domains (Figure 3.3*b*), the external magnetic field is reduced and will continue to reduce as the single domain is further

divided as shown in Figure 3.3*c*. Figure 3.3*d* shows the domain structure for a single crystal material.

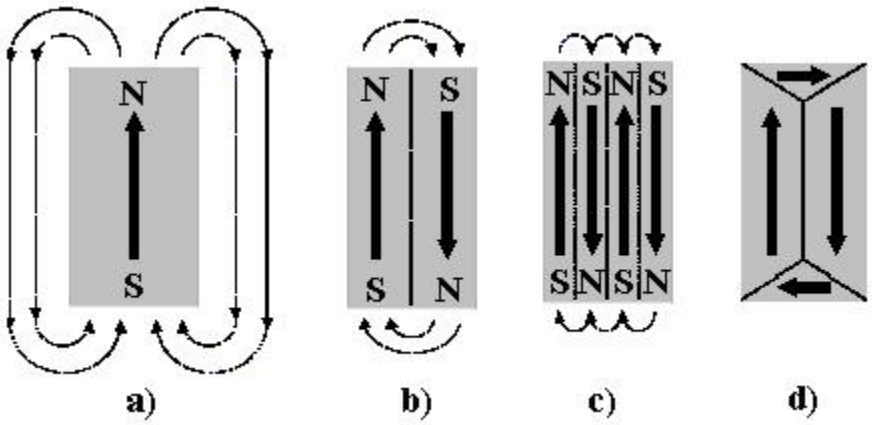

Figure 3.3 Representation of magnetic domains a) Single domain; b) Two domains; c) Four domains and d) Closure domain.

The boundary between adjacent magnetic domains is called a domain wall, which is a transition from the direction of the magnetic moments in one domain to the direction of the magnetic moment in the neighbor domain (see Figure 3.4*a*); the wall domain is usually 100 atoms wide. The width of a domain wall is due to a balance between the exchange energy and the magnetocrystaline anisotropy energy. The exchange energy is associated with interactions among atomic moments and it is minimized as the difference in orientation between dipoles is smaller (minimum with all spins parallel). The magnetocrystaline anisotropy energy is associated with tendency for the magnetic moments to align in certain directions due to crystal symmetry, stress, etc. and it increases as the domain wall becomes wider. Magnetocrystalline anisotropy energy is the energy necessary to deflect the magnetic moment in a single crystal from the easy to the

hard magnetization directions. The equilibrium domain wall width will be reached when the sum of the exchange and the magnetocrystaline anisotropy energies is a minimum (see Figure 3.4*b*).

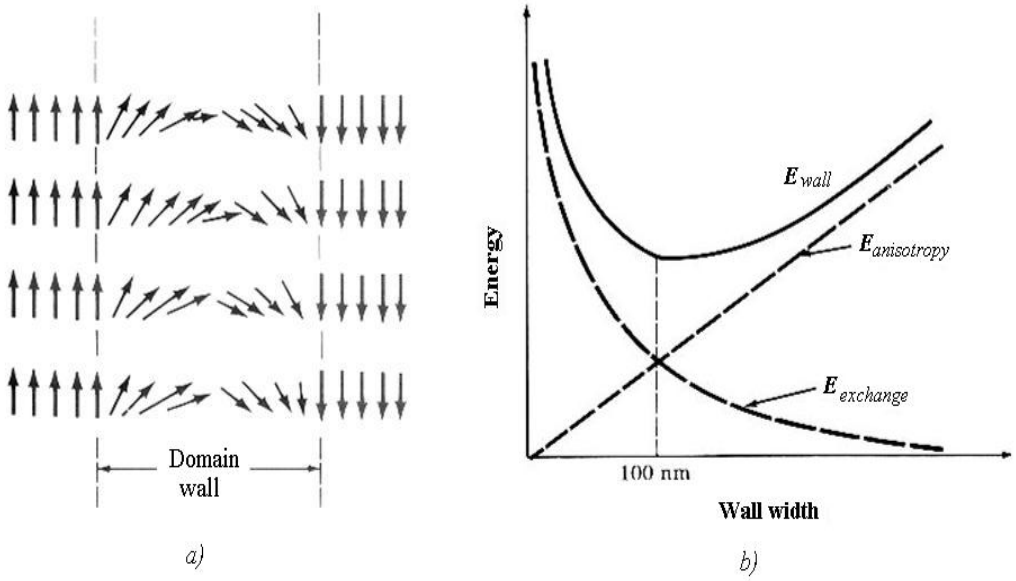

Figure 3.4 Domain wall and domain wall energy.

In the presence of a magnetic field, a demagnetized ferromagnetic material will become magnetized first by domain growth from those domains whose moments are closely aligned to the applied field. Then after domain growth finishes domain rotation towards the direction of the applied field occurs. Domain wall growth requires less energy than domain rotation and it takes place by domain wall movement as indicated in Figure 3.5. When the applied magnetic field is removed the material remains magnetized but some magnetization is lost because domains tend to rotate back to their original position.

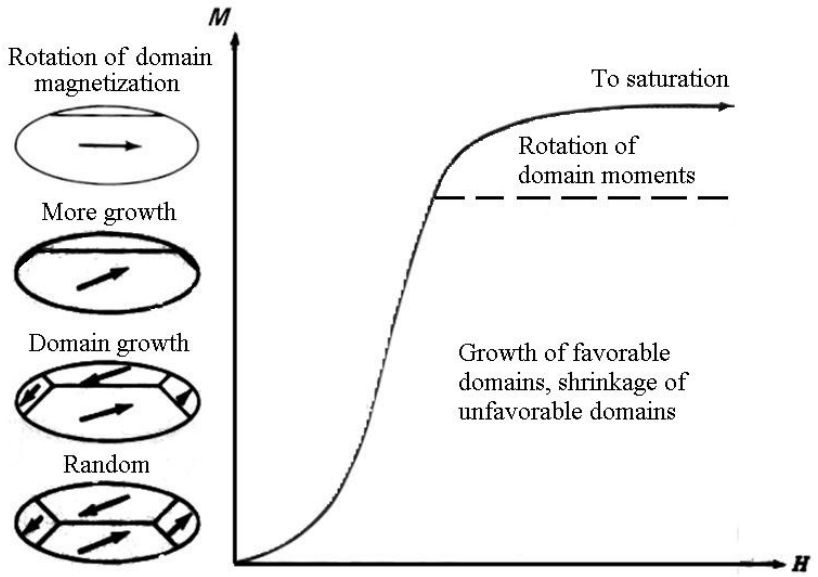

Figure 3.5 Magnetic domain growth and rotation in the presence of an external magnetic field.

3.3 Temperature Effect on Magnetization

As the temperature increases, thermal oscillation competes with the tendency for the magnetic dipoles to position themselves in a specific way. When the temperature rises beyond a certain point, the material can no longer maintain its intrinsic domain formation and becomes paramagnetic. Two temperatures are used to mark these transitions: the Curie temperature and the Néel temperature.

3.3.1 The Curie temperature

The temperature at which the ferromagnetic behavior is lost and the material starts to behave as a paramagnetic material is called the Curie temperature; Table 3.1 shows some examples of Curie temperature for various materials.

Material	Curie temperature (K)
Gadolinium	292
Nickel	631
Magnetite	858
Iron	1043
Cobalt	1393

Table 3.1 Curie temperature of selected materials

Above the Curie temperature the magnetic susceptibility of the paramagnetic material follows the Curie-Weiss law:

$$\chi = \frac{C}{T - T_C} \qquad \textbf{3.1}$$

Where C is a constant and T_C is the Curie temperature. The Curie temperature gives an idea of the amount of energy needed to break up the domain long-range ordering in the material. A universal curve of domain magnetization as function of temperature is illustrated in Figure 3.6. Not all materials follow a universal curve.

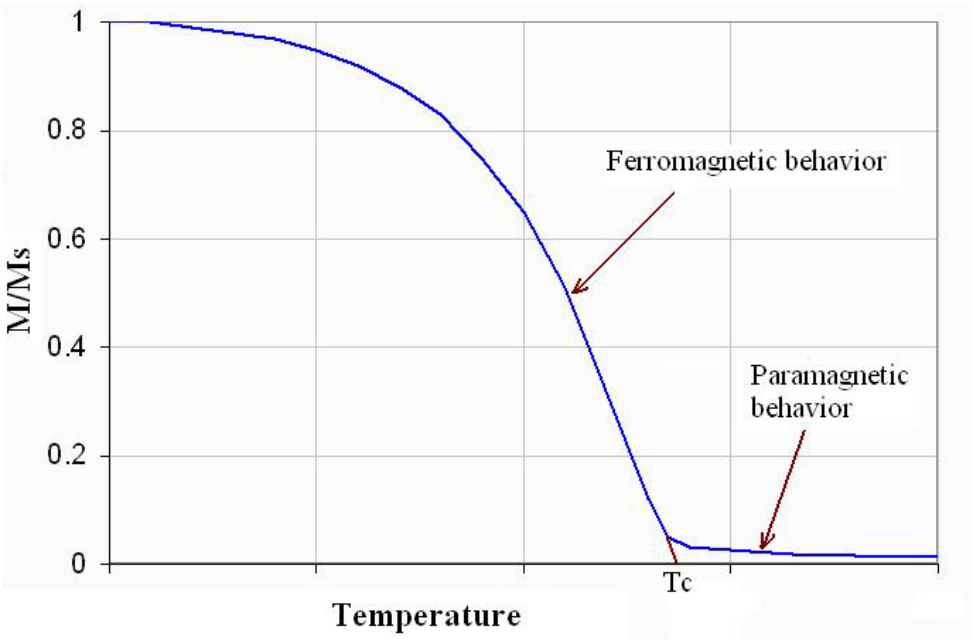

Figure 3.6 Domain magnetization as a function of temperature

Near the Curie temperature the magnetization can be assumed as a linear function of the temperature [2]; with this assumption the magnetization can be found from equation 3.2, as:

$$M = K(T_C - T) \qquad \textbf{3.2}$$

Where K is the pyromagnetic coefficient defined as:

$$K = -\frac{\partial M}{\partial T} \qquad \textbf{3.3}$$

From equation 3.2 it can be seen that the Curie temperature can be obtained from a domain magnetization vs. temperature curve by extrapolating the linear behavior of the curve to the value that intercepts the temperature axis (see Figure 3.6). This is an easy

procedure to give an approximate value of the Curie temperature but it is not precise. Another method is to find the intersection point of the two tangents that bounds the Curie temperature; one tangent corresponding to the ferromagnetic behavior and the other to the paramagnetic behavior [38]. Other suggested way to find the Curie temperature is to find the point of maximum curvature from the domain magnetization vs. temperature curve; for this procedure the measured data is differentiated twice to produce (d^2M/dT^2); the maximum value from the second derivative corresponds to the maximum curvature point and this gives a good estimate of the Curie temperature ([38],[39]). Additional information can be found in [40] - [42].

3.3.2 The Néel Temperature

The Néel temperature marks the transition from antiferromagnetic to paramagnetic behavior and as the Curie temperature is a characteristic of the material. Figure 3.7 shows the magnetic susceptibility, χ, of ferromagnetic, paramagnetic and antiferromagnetic materials as function of temperature; the turning point to paramagnetic behavior is clearly visible for both ferromagnetic and antiferromagnetic materials.

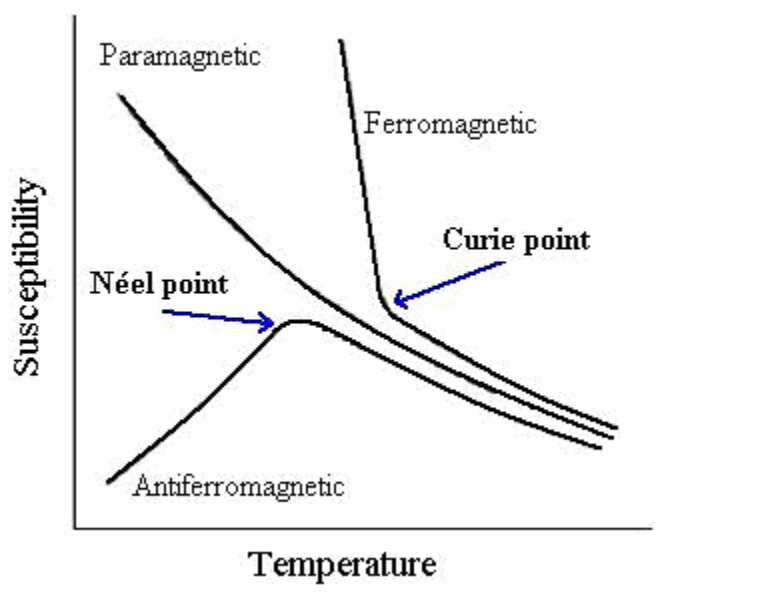

Figure 3.7 Representation of the susceptibility as a function of temperature for ferromagnetic, paramagnetic and antiferromagnetic materials.

3.4 Magnetic Fluids and Their Application

Magnetic fluids or ferrofluids are colloidal dispersions of magnetic nanoparticles in a liquid carrier. These nanoparticles have a specific size range in order to remain suspended in the liquid, about 3 to 15 nm. In this range Brownian motion (thermal molecular motion in the liquid) keeps the particles from settling out. Because magnetic particles tend to aggregate, and aggregates sediment faster than single particles, the particles are coated with a stabilizing dispersing agent. The surfactant must be matched to the carrier type and must overcome the attractive van der Waals and magnetic forces between the particles to prevent agglomeration even when a strong magnetic field is applied to the ferrofluid.

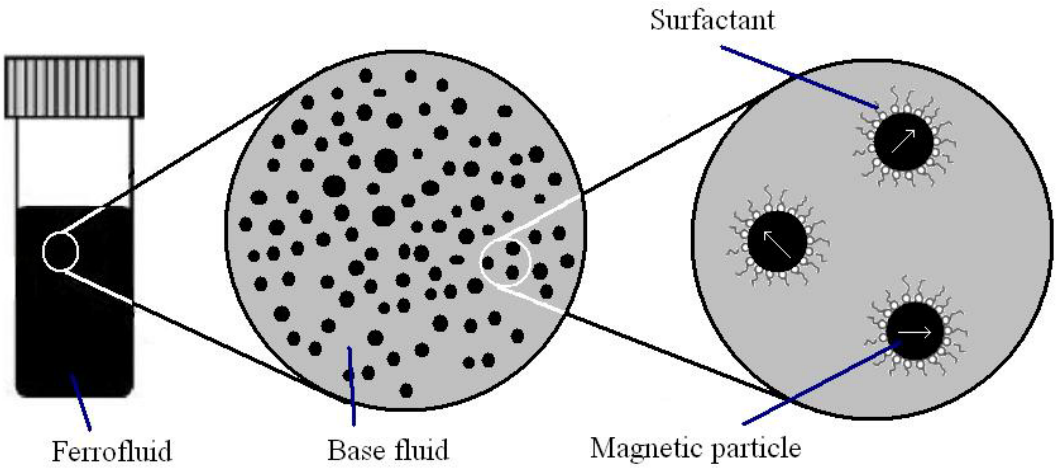

Figure 3.8 Representation of ferrofluid.

Because of their size, nanoparticles have a single magnetic domain with ferromagnetic or ferrimagnetic behavior in the molecular scale, but with zero coercivity and remanence in the colloidal scale much more like a paramagnet; this behavior is called superparamagnetic because is similar to a paramagnet but with a much larger magnetization.

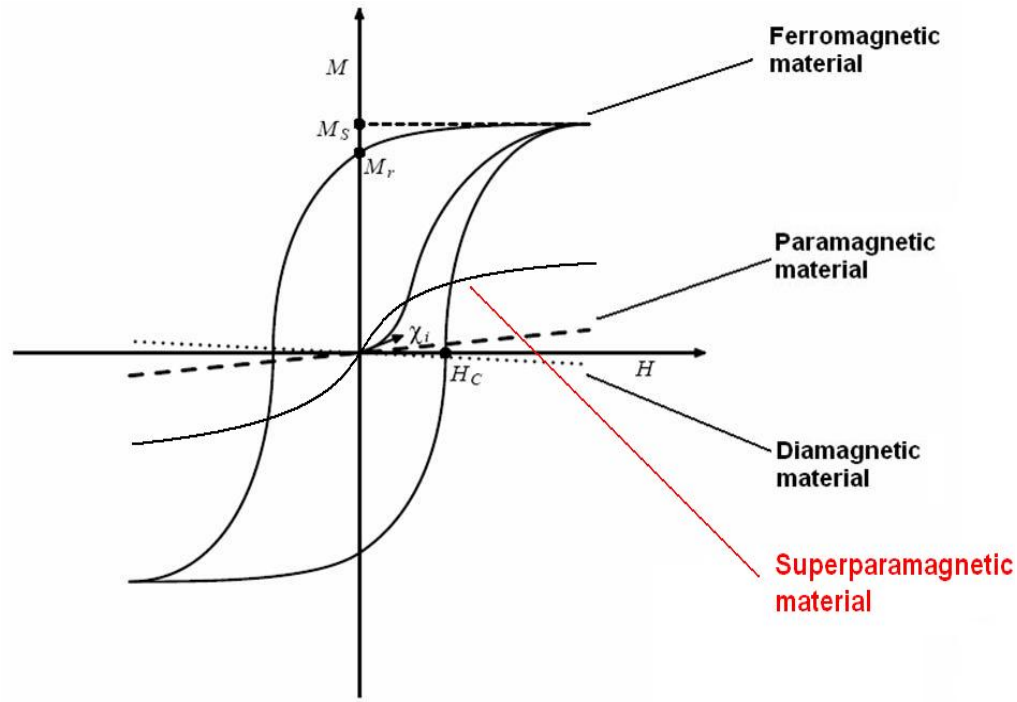

Figure 3.9. Magnetization curve for different types of materials including superparamgnetic behavior.

3.4.1 Magnetic fluids applications

Magnetic fluids are not found in nature and a synthesis process is needed. Many applications have arisen since ferrofluids were first produced by Papell in the 60s [43], the most common applications are as sealing for rotary shafts and bearings and for cooling of loud speakers; here the fluid is located in a desired position using permanent magnets [44],[45]. Other field that currently has important research interest is bioengineering; two of the most representative applications here include cancer treatment by magnetic hyperthermia and drug targeting in which thermal effects are induced by an alternating magnetic field [46]. Possible applications under investigation include magnetically controlled thermosyphons and the cooling of high power electric

transformers where the main objective is to improve the thermal performance of these devices [47].

3.5 Magnetic Fluid Synthesis

The proposed magnetic fluid, $Mn_xZn_{1-x}Fe_2O_4$, is chosen because it has been reported to have a low Curie temperature between 75°C and 325°C [8]. The ideal nanoparticle should have a Curie temperature near the maximum operating temperature of the system (100°C). Most commercially available ferrofluids are based on magnetite particles with a Curie temperature of 585°C which makes them undesirable for applications operating at temperatures near ambient temperature.

3.5.1 Magnetic nanoparticle synthesis

The synthesis of Mn-Zn ferrite is carried out by the conventional co-precipitation method; this is the most commonly method used today among the size-reduction and the microbial synthesis methods [8]. Size-reduction was the first method used to synthesize nanoparticles. In this process size reduction is carried out in a ball mill grinder under the presence of a surfactant and for a period of approximately 1000 hours, the final size of the particles is about 10 nm; the drawback of this method is the long process time. Microbial syntesis is a new approach that uses bacteria to reduce iron oxyhydroxides to nanometer-sized magnetic iron oxides, particle size and morphology are very consistent and the process is very scalable. In the co-precipitation method, a solution containing

Fe(III) and a divalent metal cation M(II), at suitable mole ratios is mixed with a hot alkaline solution. The hydrolysis reaction leads to the formation of a mixed paramagnetic Fe-M hydroxide, which undergoes dehydration and atomic rearrangement conductive to stoichiometric ferrite structure without the need of further annealing, according to:

$$2Fe^{3+} + M^{2+} + 8OH^{-} \rightarrow Fe_2M(OH)_8 \rightarrow MFe_2O_4 + 4H_2O \qquad \textbf{3.4}$$

In our case, suitable weights of Zn(II), Mn(II) and Fe(III) salts are used to get different values of "x" in the $Mn_xZn_{1-x}Fe_2O_4$ systems.

Initial molar proportion of Zn(II), Mn(II) and Fe(III) salts are taken to maintain the stoichiometric relation from equation 3.4; so it follows:

$$\frac{([Mn]+[Zn])}{[Fe]} = 0.5 \qquad \textbf{3.5}$$

Then for a certain amount of Fe(III) used, the amount of Mn(II) plus Zn(II) is fixed. The composition "x" of the ferrite nanoparticles is obtained from the relation of Mn(II) to complete metal cation Mn(II) plus Zn(II):

$$x = \frac{[Mn]}{([Mn]+[Zn])} \qquad \textbf{3.6}$$

Initial molar proportion of the coprecipitating agent does not maintain the stoichiometric relation of equation 3.4 and excess of OH^- is used,; the amount of the base and its concentration are determined experimentally [48].

The nucleation rate is quite high at the beginning of the process whereas the excess of OH^- ions provides a net negative surface charge to the nuclei limiting their further growth and aggregation. Under these conditions polydisperse particles of less than 50nm in diameter are typically produced [49].

For the synthesis of the $Mn_xZn_{1-x}Fe_2O_4$ particles the metallic salt used are: Iron(III) chloride Hexahydrate ($FeCl_3.6H_2O$), Manganese(II) chloride Tetrahydrate ($MnCl_2.4H_2O$) and Zinc chloride ($MnCl_2$). The based used is Sodium hydroxide (NaOH). The metallic salt solution has an iron concentration of 0.11mol/L and the base solution has a concentration of approximately 0.5mol/L. A schematic of the magnetic nanoparticle synthesis is presented in Figure 3.10, the reaction time for the formation of ferrite nanoparticles under constant volume and heating is 4 hours. Reaction time and hydroxide (OH^-) excess were established experimentaly by Perales et al. [48].

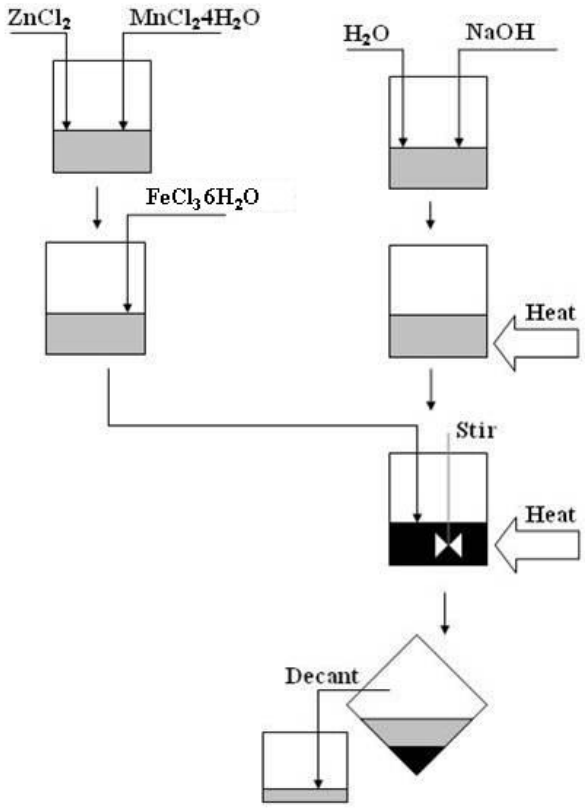

Figure 3.10 Schematic of the synthesis process of magnetic nanoparticles.

3.5.2 Magnetic nanoparticle suspension

The suspension process includes cleaning, surfactant coating or particle electrostatic charge, and the addition of a base fluid. The cleaning process was carried out using two different cleaning solutions: distilled water and nitric acid with a concentration of 2mol/L. After the nanoparticles are produced and the supernatant is decanted the cleaning solution is poured into the container and the mixture is agitated for about 10 minutes; then the mixture is centrifuged at 3500 rpm and the liquid is decanted from the mixture. The cleaning process is repeated three times.

Two surfactant agents were used: tetramethylammonium hydroxide and oleic acid; the later did not work well and only ferrofluid with very low concentration was produced therefore it was not further analyzed. The tetramethylammonium hydroxide is used diluted in a solution of 25% tetramethylammonium hydroxide and 75% water, so in this case surfactant coating and addition of a base fluid are coupled together; this surfactant provides a negative charge in the surface of the nanoparticles to inhibit their aggregation [24]. The surfactant is added into the nanopaticles by small amounts, usually 1 ml, to try to achieve maximum concentration. The mixture, of surfactant solution and nanoparticles, is agitated for 10 minutes and centrifuged for 5 minutes at 1200 rpm; the fluid remaining on top of precipitated nanoparticles is the ferrofluid.

When nitric acid solution is used as the cleaning agent it creates a positive electrostatic charge in the nanoparticles that prevents the particles from sticking to each other; the use of surfactant is not needed and the base fluid is applied directly after the cleaning process. The properties of the produced nanopartilces and the ferrofluid are presented in the next chapter.

4 CHARACTERIZATION OF NANOPARTICLES AND MAGNETIC FLUID

4.1 Nanoparticle Characterization

4.1.1 Composition

After the nanoparticles are obtained a composition analysis was carried out to corroborate that the product of the process is in fact what is supposed to be ($Mn_xZn_{1-x}Fe_2O_4$), and that the chemical reaction in the coprecipitation process was complete. An X-ray diffractometer is used to verify that the crystalline structure of the produced nanoparticles match the patterns of a ferrite structure. Each crystalline solid has its unique characteristic X-ray pattern which is used for its identification. X-ray diffraction patterns of $Mn_xZn_{1-x}Fe_2O_4$ powders, produced after 5 hours of reaction time and for different compositions (different values of x) are shown in Figure 4.1. The vertical axis of the plot represents the X-ray intensity, the horizontal axis is the measured angle (2θ). The measured peaks in the graph correspond to a specific crystallographic plane of the ferrite structure. From the analysis of the peaks the formation of the ferrite structure can be verified.

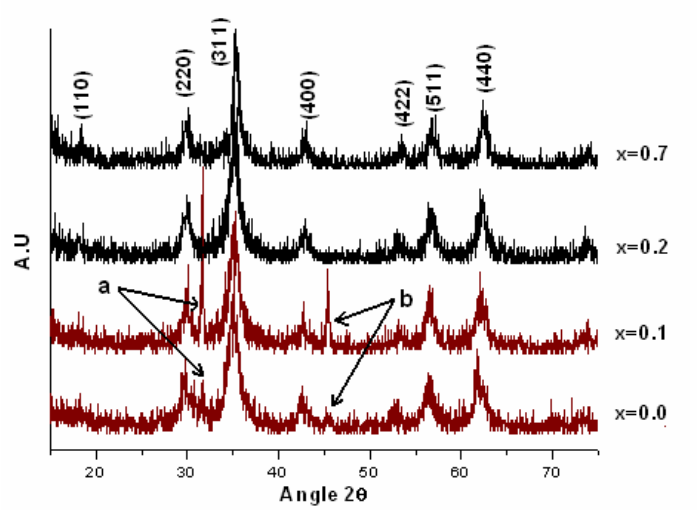

Figure 4.1 X-Ray Diffraction patterns for $Mn_xZn_{1-x}Fe_2O_4$ particles for various x; adapted from [48].

From the x-ray analysis it can be inferred that the presence of Zn ions delayed the formation of the ferrite structure; peaks for x= 0.0 and x=0.10 at 31 and 46 angle 2θ, marked as **a** and **b**, suggest the incomplete formation of the corresponding structure. For values of x=0.2 and x=0.7 the x ray pattern of the ferrite powders match the composition of the ferrite structure [48].

4.1.2 Saturation magnetization

To continue with the characterization of the nanoparticles their magnetic behavior were measured, for this purpose a SQUID (Superconducting Quantum Interference Device) magnetometer is used. The measurements were carried out at a temperature of 300 K and the maximum applied magnetic field is 45 KOe. The results for different compositions of $Mn_xZn_{1-x}Fe_2O_4$ are shown in Figure 4.2.

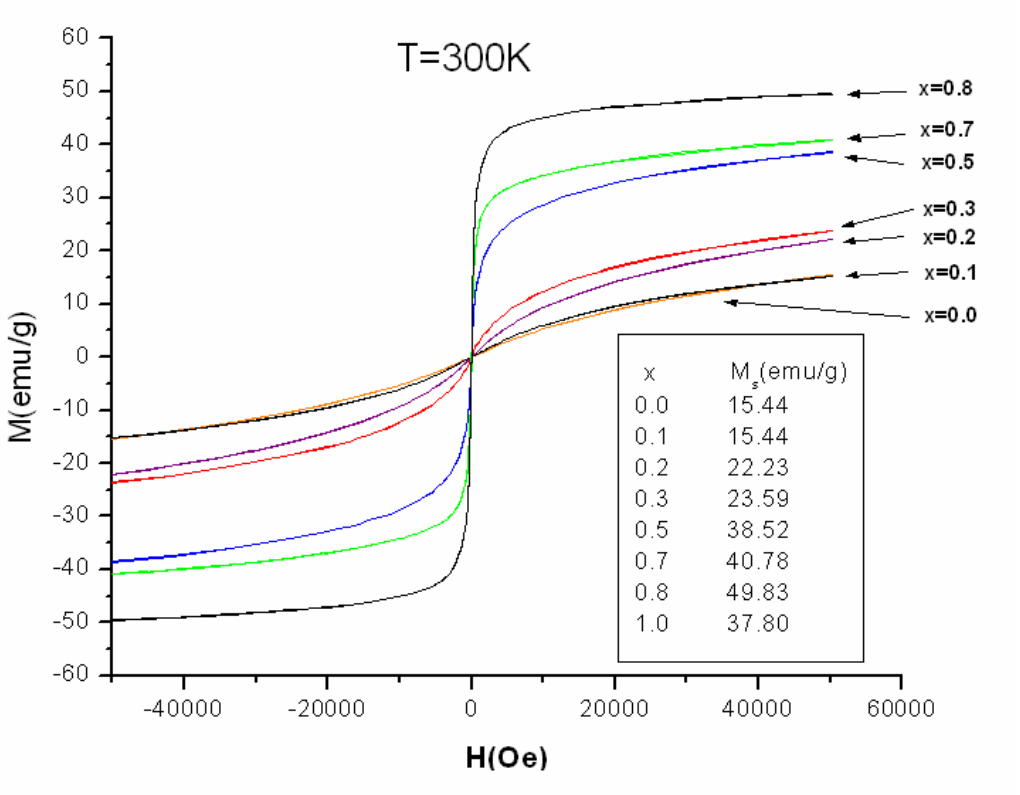

Figure 4.2 Comparison of M-H curves at room temperature for different fractions of Manganese [48].

As can be seen, produced $Mn_xZn_{1-x}Fe_2O_4$ exhibited a superparamagnetic behavior at room temperature; the saturation magnetization and saturation conditions were strongly dependent on the composition. The substitution of Mn^{2+} for non-magnetic Zn^{2+} ions (for the given 'x' values) explains the observed increasing trend in saturation magnetization with 'x', reaching a maximum saturation magnetization with x=0.8. Ferrites with x=0.5, x=0.7 and x=0.8 are chosen for suspension in the base fluid since these nanoparticles show the best magnetic behavior.

4.2 Ferrofluid Characterization

The desired characteristics of the magnetic fluid for the operation of the magnetocaloric pump are low Curie temperature, high magnetization, high pyromagnetic coefficient, high thermal conductivity and low viscosity. The measurements of these properties are presented next.

4.2.1 Physical properties

The weight concentration and volumetric concentrations are measured experimentally by weighing a fixed amount of ferrofluid and measuring its volume and then evaporating the base fluid and the surfactant and weighing the nanoparticles, finally adding a fix amount of water and measuring the volume change to determine the exact volume of the nanoparticles. The density of the nanoparticles and that of the ferrofluid are calculated from these measurements. The results are presented in Table 4.1

Manganese fraction x	**Volume concentration (%)**	**Weight concentration (%)**	**Nanoparticle density (Kg/m^3)**	**Ferrofluid density (Kg/m^3)**
0.5	2.20	10.1	5398	1087
0.7	1.34	6.39	5237	1052
0.8	1.84	8.59	5279	1073

Table 4.1 Some physical properties at different composition of $Mn_xZn_{1-x}Fe_2O_4$ ferrofluid.

Samples with equal volumetric concentration (ϕ=1.34%) are prepared by addition

of water to the more concentrated ferrofluids (x=0.5 and 0.8) for comparison purposes. Also ferrofluids with different concentration are synthesized and analyzed to determine the effect of nanoparticle concentration on the fluid properties.

The viscosity of nanofluids depends on temperature, interaction between particles, concentration, shape and dimensions of the particles and the viscosity of the liquid carrier. Approximate relationships have been proposed but these have not been able to account for all the phenomena parameters so there is no general formula for the viscosity of magnetic fluids [50]. The viscosity measurements are carried out using commercially available equipment. Measurements of viscosity at 25°C are presented in Figure 4.3. as can be seen the fluid is Newtonian (constant shear rate) with a dynamic viscosity ranging from 0.00135 Pa s for the low concentration ferrofluid (ϕ=0.45%) to 0.00145 Pa s for medium concentration (ϕ=2.2%).

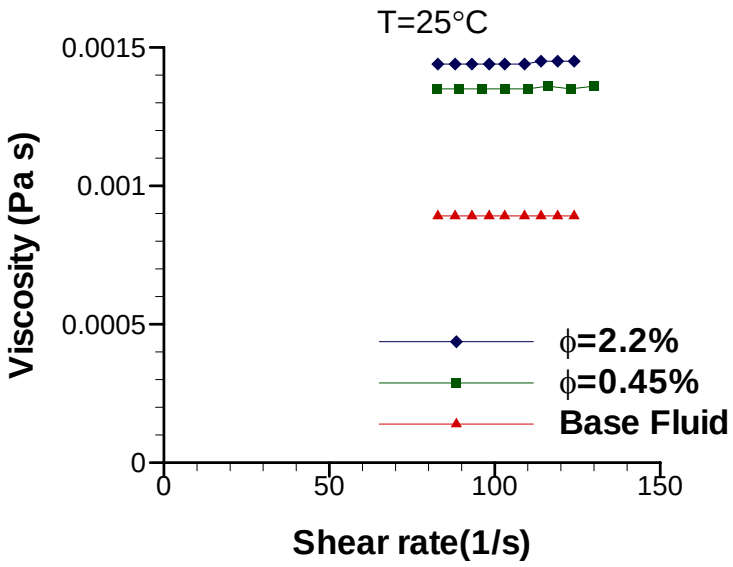

Figure 4.3 Dynamic viscosity of various ferrofluids

4.2.2 Magnetic Properties

Saturation magnetization M_s and magnetization M vs. temperature were measured using a SQUID magnetometer; the results are presented next. Figure 4.4 is obtained by placing the ferrofluid in the SQUID, setting a constant temperature of 300K and measuring the magnetization of the sample as the magnetic field is being increased from 0 to 50 KOe.

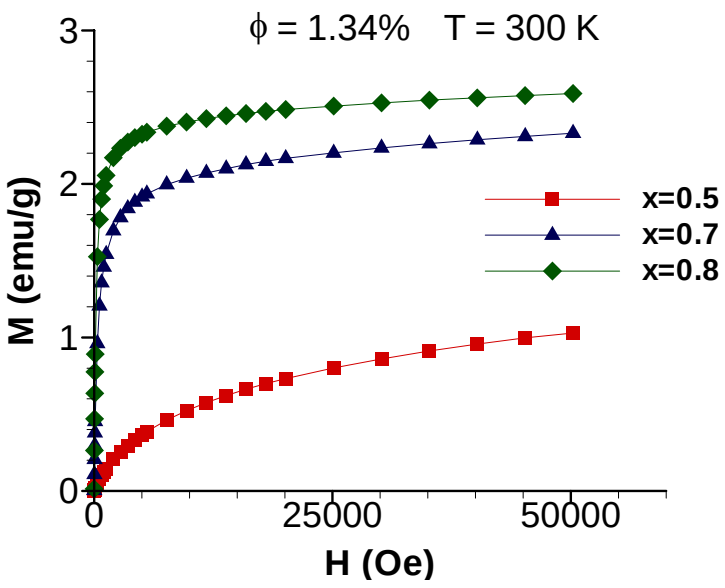

Figure 4.4 Magnetization curve for different composition of $Mn_xZn_{1-x}Fe_2O_4$ ferrofluid.

From Figure 4.4 it is clear that the ferrite with composition x=0.7 and x=0.8 have similar magnetic behavior, with similar initial susceptibility χ and reach saturation magnetization at similar applied magnetic field with x=0.8 having a higher magnetization than x=0.7. For x=0.5 the behavior is different with lower initial susceptibility χ and saturation magnetization much lower than the other two samples. To analyze the effect of particle concentration additional samples are synthesized and the magnetization measurements are repeated. Figure 4.5 shows the magnetic behavior of ferrofluid with x=0.5 for three different concentrations.

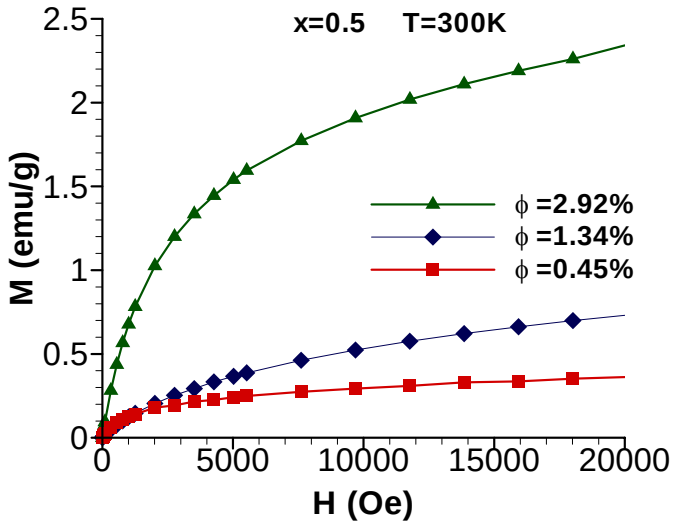

Figure 4.5. Magnetization curve for different volumetric concentration of $Mn_{0.5}Zn_{0.5}Fe_2O_4$ ferrofluid.

From Figure 4.5 can be seen that the effect of concentration has a great influence on the magnetic behavior of the ferrofluid. Higher concentrations have better magnetic properties are obtained, namely higher initial susceptibility and higher saturation magnetization.

Measurements of the effect of temperature on the magnetization are performed by setting a constant magnetic field and measuring the magnetization of the ferrofluid at different temperatures. Figure 4.6 shows ferrofluids with different composition and the same concentration at a magnetic field of 20 KOe. Figure 4.7 shows the same samples at different applied magnetic fields.

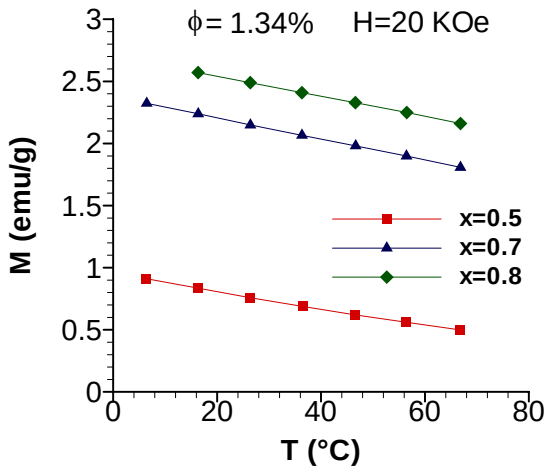

Figure 4.6 Magnetization vs. Temperature for different composition of $Mn_xZn_{1-x}Fe_2O_4$ ferrofluid at a magnetic field of 20000Oe

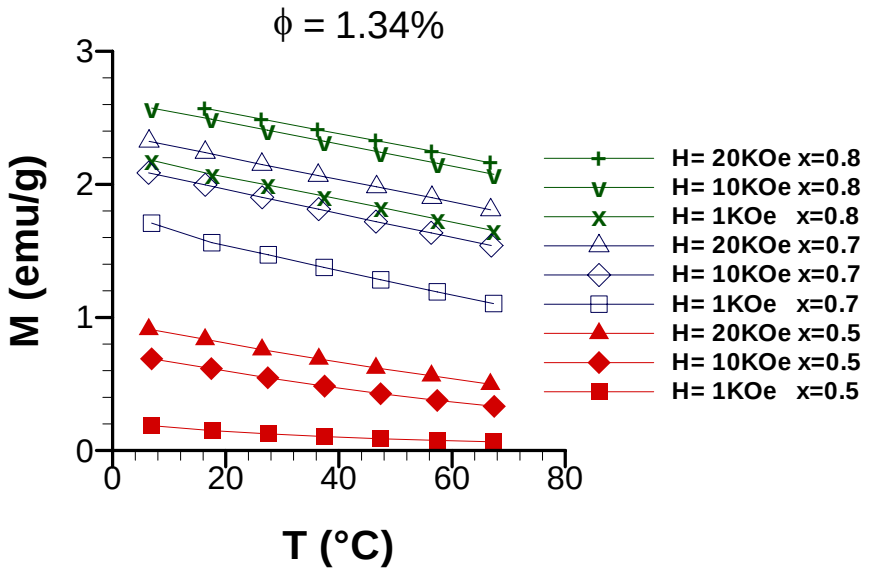

Figure 4.7 Magnetization vs. Temperature for different composition of $Mn_xZn_{1-x}Fe_2O_4$ ferrofluid and different magnetic fields.

Figure 4.6 shows a similar pyromagnetic coefficients ($\partial M/\partial T$) and a linear behavior throughout the temperature range used for the three samples; while in Figure 4.7

can be seen that at smaller magnetic fields (1000 Oe) x=0.5 and x=0.7 are not perfectly linear; indicating that the pyromagnetic coefficients varies with the magnetic field. The effect of particle concentration is also analyzed and the results are presented in Figure 4.8.

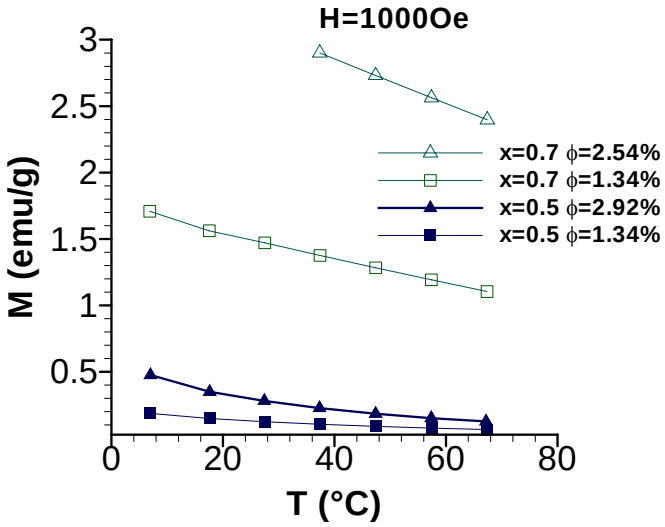

Figure 4.8 Magnetization vs. Temperature for different volumetric concentrations of $Mn_xZn_{1-x}Fe_2O_4$ ferrofluid.

As can be seen from Figure 4.8, the composition and the concentration of the nanoparticles have a strong impact in the magnetization of the ferrofluid.

To estimate the Curie temperature of the ferrofluid an extrapolation of the data shown in Figure 4.8 is carried out to find the intercept with the temperature axis. This procedure is valid for small applied magnetic fields because the magnetization of the paramagnetic material at small fields is close to zero. To obtain a more precise value for

the Curie temperature a similar procedure should be performed on the solid particles for a wider temperature range. A wider temperature range should allow to establish the transition from ferro or ferrimagnetic behavior to paramagnetic behavior as described in Chapter 3. Values obtained from these plots are presented in Table 4.2.

Manganese composition x	**ϕ (%)**	**Pyromagnetic coefficient *K* (A/m °C)**	**Estimated Curie temperature (°C)**
0.5	2.91	8.95	79.4
0.7	2.54	20.1	210.3
0.8	1.54	13.1	175.9

Table 4.2 Curie temperature and pyromagnetic coefficient for produced ferrofluids.

From the obtained data can be seen that the ferrofluid with the lowest Curie temperature does not have the highest pyromagnetic coefficient and in fact the highest pyromagnetic coefficient is displayed by the ferrofluid with the highest Curie temperature, $Mn_{0.7}Zn_{0.3}Fe_2O_4$. Also from these measurements, it can be seen that the Curie temperature varies dramatically from one sample to another.

4.2.3 Particle size from magnetic measurements

Particle size estimation is carried out from the magnetization data of the suspended nanoparticles from the asymptotic values of the Langevin function (equation

4.1) for small and large values of the parameter α [2].

$$\frac{M}{\phi M_d} = \coth\alpha - \frac{1}{\alpha} \equiv L(\alpha) \qquad \textbf{4.1}$$

Where:

$$\alpha = \frac{\pi}{6}\frac{\mu_0 M_d H d^3}{kT} = \frac{mH}{kT} \qquad \textbf{4.2}$$

M is the magnetization of the ferrofluid, ϕ is the volume fraction of magnetic solids, M_d is the saturation moment of the bulk magnetic solid, the parameter μ_0 is the permeability of the free space with a value $\mu_0 = 4\pi\times10^{-7}$ H/m, H is the applied magnetic field, d is the diameter of the nanoparticles, k is the Boltzmann constant with a value of $k = 1.38\times10^{-23}$ N m/K, T is the absolute temperature and m is the particle magnetic moment. For small values of α (small applied magnetic field H), the initial susceptibility of the ferrofluid is given by:

$$\chi_i = \frac{\pi\phi\mu_0 {M_d}^2 d^3}{18kT} \qquad \textbf{4.3}$$

For large values of α (large applied magnetic field H), the particle diameter can be obtained from the asymptotic form of equation 4.1

$$\frac{M}{\phi M_d} = \left(1 - \frac{6kT}{\pi\mu_0 M_d H d^3}\right) \qquad \textbf{4.4}$$

In small magnetic fields the magnetization of the ferrofluid is governed by the

larger particles which are more easily oriented by the field; while at high magnetic fields, close to saturation magnetization of the ferrofluid, only the small particles are left to be oriented. Therefore equation 4.3 will give larger values of particles diameter than equation 4.4. The volume fraction can be calculated from:

$$M_d = \frac{M_s}{\phi} \qquad \textbf{4.5}$$

The saturation magnetization is obtained from a plot of magnetization vs. reciprocal magnetic field (*1/H*) at high fields. The data is obtained from the same measurements showed in Figure 4.4 (x= 0.5, 0.7, 0.8 with the same concentration of nanoparticles per liquid volume, at temperature of 300K). If the ferrofluid is close to its saturation magnetization the data can be assumed linear (see Figure 4.9).

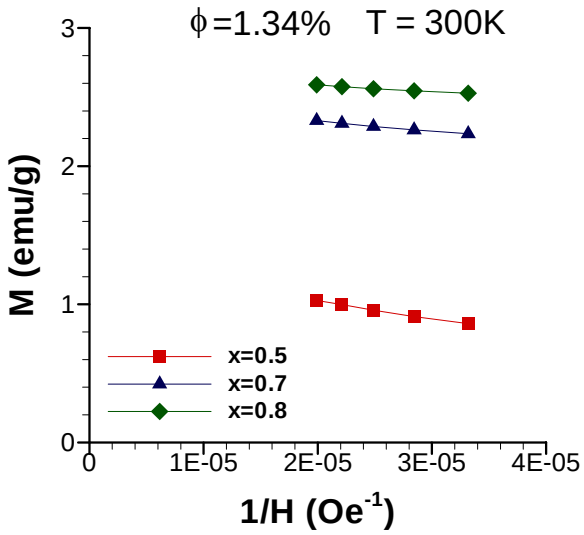

Figure 4.9 Magnetization vs. Reciprocal magnetic field at large fields

The intercept with the magnetization axis is obtained by extrapolation of the data; this value gives the magnetization of the ferrofluid at an infinite applied magnetic field. The bulk material magnetization is obtained from equation 4.5 from the measured volume fraction, with this value the nanoparticle diameter can be calculated at low and high fields; the results are presented in Table 4.3. An almost horizontal line represents that the sample is close to its saturation magnetization because an increase in magnetic field would not modify significantly the value of its magnetization. From Figure 4.7 it can be appreciated that the slopes of the samples are almost horizontal and linear. If a sample is not near its saturation magnetization the calculated diameter for small particles may not be a representative value.

Manganese composition x	**M_s (emu/g)**	**M_d (emu/g) calculated**	**M_d (emu/g) measured [48]**	**d at low fields (nm)**	**d at high fields (nm)**
0.5	0.945	19.1	38.5	7.65	4.72
0.7	2.47	37.5	40.8	14.0	6.82
0.8	2.68	41.1	49.8	17.8	8.01

Table 4.3 Calculated properties for different composition of $Mn_xZn_{1-x}Fe_2O_4$ and ϕ=1.34%.

The calculated value of the saturation magnetization of the solid particles does not agree well with the measured values. The synthesis process of the nanoparticles is the same for the measured [48] and from the calculated values. A similar value of magnetization should be expected. The lower value of magnetization of the nanoparticles may be attributed to the cleaning process involving the nitric acid solution that is carried

out to the particles before they are suspended in the base fluid. The acid solution is believed to be reacting with the Zn in the ferrite (the highest difference is obtained for the ferrofluid with highest content of Zn) producing smaller particles and therefore with lower magnetization. The particle size obtained from equations 4.3 and 4.4 present values within the expected range.

A summary of the magnetic characterization for the synthesized ferrofluids is presented in Table 4.4.

Ferrofluid composition x	**ϕ (%)**	**Density (Kg/m3)**	**Ms (emu/g)**	**Ms (A/m)**	**K (A/m °C)**	**d low fields (nm)**	**d high fields (nm)**
0.5	2.91	1119	2.72	3052	8.95	5.50	4.54
0.7	2.54	1110	4.91	5450	20.1	13.60	5.55
0.8	1.54	1061	3.10	3284	13.1	12.79	4.44
0.5	1.34	1052	0.945	994	7.15	7.65	4.72
0.7	1.34	1052	2.47	2546	10.2	14.0	6.82
0.8	1.34	1052	2.68	2819	9.05	17.8	8.01

Table 4.4 Summary of magnetic characterization of different synthesized ferrofluids.

From the measured properties and comparing with previous work is appreciable that the volumetric concentration of the synthesized ferrofluid still needs improvement ([8],[15]) but saturation magnetization for the $Mn_xZn_{1-x}Fe_2O_4$ are consisten with reported values ([13],[17],[18],[19],[20]). Particle size is between the expected range and the results agree with the data reported by Auzans et al.[13] for the effect of Zn concentration

with the particle size.

4.2.4 Thermal Properties

There are no theoretical formulas available to predict the thermal conductivity of nanofluids; existing models are proposed for large particles in the order of micrometers or higher and may be used only for a rough estimation but will not give any accurate value of the thermal conductivity of the nanofluid ([27], [51] - [55]). The lack of reliable correlations makes experimentation the only reliable way to determine these properties in such fluids. For thermal conductivity measurements the transient hot-wire method is implement, this method is commonly used for such measurements [27], [29], [51] and it is believed to be the most accurate [54]. The main advantage of this method is its almost complete elimination of natural convection effects. Another advantage is that it is fast compared with other techniques. In order to use the hot-wire technique to a ferrofluid a modification must be made because the hot-wire method can not be applied to electrical conducting fluids since part of the current passing through the hot-wire will be conducted by the fluid and the measurements will be altered [56]. To prevent the current to pass through the fluid the hot wire is covered with an electrical insulating coating. A typical hot-wire apparatus is presented schematically in Figure 4.10.

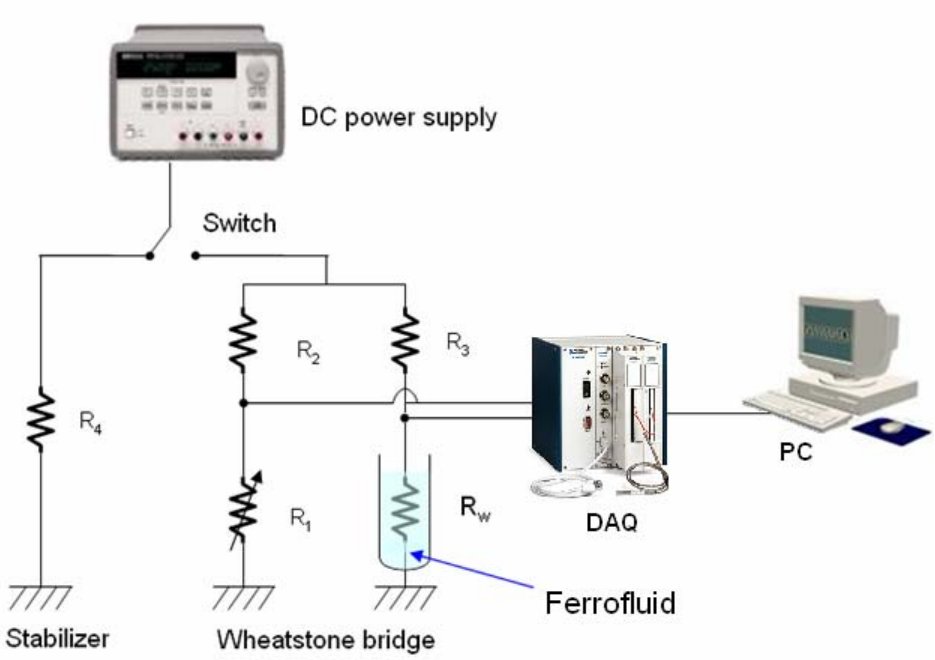

Figure 4.10 Representation of hot-wire apparatus

The hot-wire apparatus consists of a platinum wire suspended in a liquid in a vertical cylinder container; the platinum wire is used as heater and as temperature sensor. For the temperature measurement the platinum wire is used as a resistance temperature detector (RTD), because the resistivity of platinum shows highly linear temperature dependence; making it ideal for high accuracy measurements. The platinum wire is mounted in a Wheatstone bridge to improve the accuracy by reducing impedance error [57]. The basic Wheatstone bridge contains four resistances, a voltage source and a voltage meter. The circuit is said to be balanced when the reading from the voltage meter is zero and the relation between the resistances is [58]:

$$\frac{R_1}{R_2} = \frac{R_W}{R_3} \tag{4.6}$$

R_1 is a variable resistance and is set to balance the circuit initially then as current flows through the platinum wire, R_W, its resistance changes and the system becomes unbalanced. R_2 and R_3 are regular resistors. The equation for the unbalanced circuit is:

$$\frac{V_{out}}{V_{in}} = \frac{R_1}{R_1 + R_2} - \frac{R_W}{R_W + R_3} \tag{4.7}$$

Equation 4.7 can be transformed to find R_W from the measurement of output voltage V_{out}, by knowing the input voltage V_{in} and resistances R_1, R_2, R_3.

$$R_W = \frac{V_{in}R_1 - V_{out}(R_1 + R_2)}{V_{in}R_2 + V_{out}(R_1 + R_2)} R_3 \tag{4.8}$$

The resistance of the platinum wire R_W is related to the temperature by a linear regretion equation, this equation is obtained from a calibration curve by placing the platinum wire at known temperatures and measuring its resistance. The temperatures used for the calibration were 0°C (freezing point of water), 22°C (ambient temperature) and 100°C (boiling point of water). The linear regression yields:

$$T = 2.5860R_W - 256.90 \tag{4.9}$$

The measured data from the hot-wire apparatus is curved fitted using a logarithmic scale to account for any error in the data acquisition then two points are selected from the fitted curve and the thermal conductivity is obtained from equation 4.10.

$$k = C\frac{q}{4\pi(T_2 - T_1)}\ln\left(\frac{t_2}{t_1}\right) \qquad \textbf{4.10}$$

The constant C is used to correct the effect of the coating. A calibration measurement of the thermal conductivity of a known fluid is necessary. For this purpose Toluene is selected, its thermal conductivity is 0.1326W/m K [56]. Measurements to corroborate the precision of the device are presented in Table 4.5.

Fluid	**Reference value (W/m K)**	**Measured value (W/m K)**	**Deviation (%)**
Toluene	0.1326	-	-
Acetone	0.1600	0.1618	1.13
Heptane	0.1240	0.1249	0.726
Water	0.6000	0.5905	1.51

Table 4.5 Comparison between measured thermal conductivity of selected liquids and reference values.

Measurements of thermal conductivity of ferrofluids are presented in Figure 4.11. the vertical axis corresponds to the relation between the measured thermal conductivity of the ferrofluid k_{eff} and the thermal conductivity of the base fluid k_{bf}; which for the current ferrofluid is water.

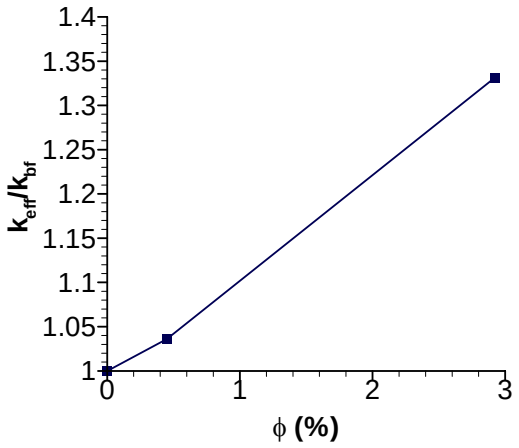

Figure 4.11 Thermal conductivity vs. volumetric concentration.

The thermal conductivity of the ferrite ferrofluid (x=0.7) is greatly influenced by the concentration of nanoparticles and the increment with respect of the conductivity of the base fluid is significant.

5 DEVELOPMENT OF A MAGNETOCALORIC PUMP FOR APPLICATIONS IN HEAT PIPES.

5.1 Background

A brief description of a heat pipe and a magnetocaloric pump are presented in the following paragraphs.

A heat pipe is one of the most efficient systems, to transport heat; among its advantages are the capacity to transport large amounts of heat through a small cross-sectional area over a relative large distance with a small end to end temperature drop and the possibility to transport and control high heat rates at different temperatures [4]. The heat transfer capacity of heat pipes operating from 200 to 550K is limited mostly by the capillary limit, which occurs when the pumping rate of liquid is not enough to keep the evaporation section with fluid [5]. To improve this limitation different types of heat pipes have been developed including loop heat pipes and capillary pumped loops which represent the major thermal control innovation of the last decade [59]; these types of heat pipes have some draw backs including difficult start up condition because the liquid an vapor phase have to be located properly inside the loop and it is not always guaranteed from their initial condition. Due to their major cost; capillary pumped loops use is restricted to applications in space or special areas where cost is not a major concern.

The basic mechanism for power generation in a magnetocaloric pump consists of a region where a magnetic fluid experiences a temperature increase while being exposed to a magnetic field. The magnetic fluid experiencing a temperature increase approaches the Curie temperature and its magnetization decreases, losing its attraction from the magnetic field and therefore being displaced by colder magnetic fluid that has not yet been exposed to the heating source ([2]; [8]). To give a general description of the pressure generated in a magnetocaloric pump, the ferrohydrodynamic (FHD) Bernoulli equation is presented.

5.1.1.1 The ferrohydrodynamic Bernoulli equation

The ferrohydrodynamic Bernoulli equation for steady state under the assumptions of incompressible, inviscid liquid, without hysteresis, collinear magnetization and magnetic field, irrotational flow, constant gravitational force and either isothermal flow field or temperature independent magnetization; is:

$$p^* + \frac{1}{2}\rho v^2 + \rho g h - \mu_0 \bar{M} H = C \qquad \textbf{5.1}$$

Where C is a constant and p* is the composite pressure defined as:

$$p^* = p(\rho, T) + \mu_0 \int_0^H \upsilon \left(\frac{\partial M}{\partial \upsilon} \right)_{H,T} dH + \mu_0 \bar{M} H \qquad \textbf{5.2}$$

$\bar{M}$ is the field-average magnetization defined as:

$$\bar{M} = \frac{1}{H}\int_0^H M dH \qquad \textbf{5.3}$$

Equation 5.1 can be obtained from the general Navier-Stokes equation that includes the magnetic body force $\mu_0 M \nabla H$ and using the composite pressure instead of pressure as:

$$\rho \frac{Dv}{Dt} = -\nabla p^* + \rho g + \mu_0 M \nabla H \qquad \textbf{5.4}$$

The FHD Bernoulli equation can not be applied to the region in the magnetocaloric pump where the fluid is increasing its temperature but it can be applied before and after this region; Figure 5.1 shows the sections where the magnetocaloric pump is divided in order to apply the FHD Bernoulli equation. Section 1 and 4 are chosen at a location where the magnetic field can be neglected and section 2 and 3 enclose a practically uniform magnetic field.

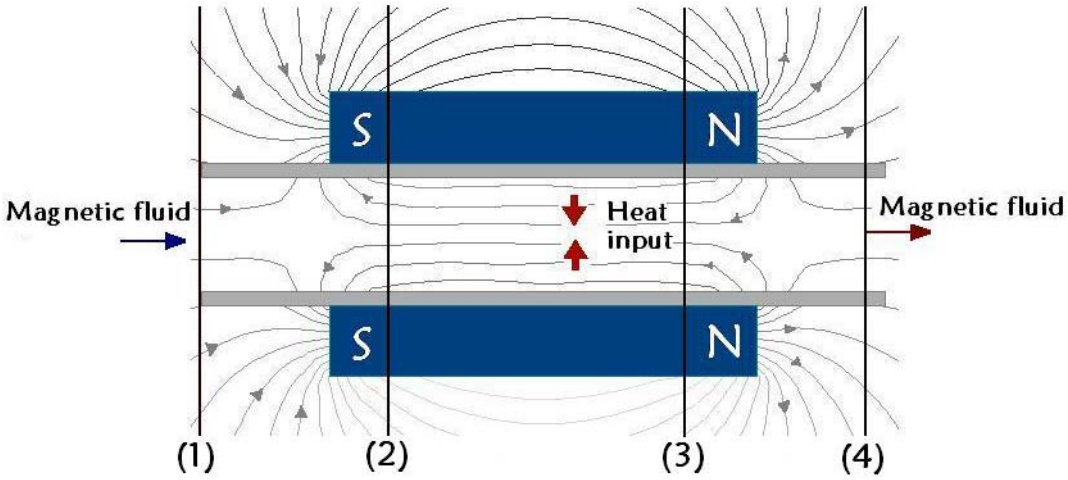

Figure 5.1 Magnetocaloric pump divided into different sections for application of the FHD Bernoulli equation.

For a constant cross sectional pipe (constant kinetic energy) and neglecting any change in potential energy, the FHD Bernoulli equation 5.1 between sections 1 and 2 (as shown in Figure 5.1) can be simplified to:

$$p^*_1 = p^*_2 - \mu_0(\bar{M}H)_2 \qquad \textbf{5.5}$$

Following the same reasoning, the FHD Bernoulli equation between sections 3 and 4 is:

$$p^*_3 - \mu_0(\bar{M}H)_3 = p^*_4 \qquad \textbf{5.6}$$

In sections 1 and 4 the magnetic field is negligible so the composite pressure reduces to:

$$p^*_{1,4} = p(\rho,T)_{1,4} \qquad \textbf{5.7}$$

And considering Equation 5.4 inside the magnetic field (between sections 2 and 3) where the FHD Bernoulli equation can not be applied; neglecting acceleration of the fluid ($\frac{Dv}{Dt} = 0$), friction ($\eta = 0$) and gravity, it is clear that:

$$0 = -\nabla p^* + \mu_0 M \nabla H \qquad \textbf{5.8}$$

Since the magnetic field between sections 2 and 3 is uniform $\nabla H=0$ and therefore:

$$p^*_2 = p^*_3 \qquad \textbf{5.9}$$

Substituting equation 5.5 into equation 5.6 the change in pressure between section 4 and 1 can be obtained:

$$p_1 + \mu_0(\bar{M}H)_2 - \mu_0(\bar{M}H)_3 = p_4$$

$$p_4 - p_1 = \mu_0 H[\bar{M}(T_2) - \bar{M}(T_3)] \qquad \textbf{5.10}$$

$$\Delta p = \mu_0 H \Delta \bar{M}$$

The possibility for transforming heat into mechanical energy using a ferrofluid has been demonstrated; practical considerations for the operation of the magnetocaloric pump are presented next.

5.1.1.2 Operational temperature

As indicated in chapter 1 the magnetization of the ferrofluid is a function of the temperature and as the ferrofluid approaches its Curie temperature the change in magnetization is greater for a given change in temperature (Figure 5.2).

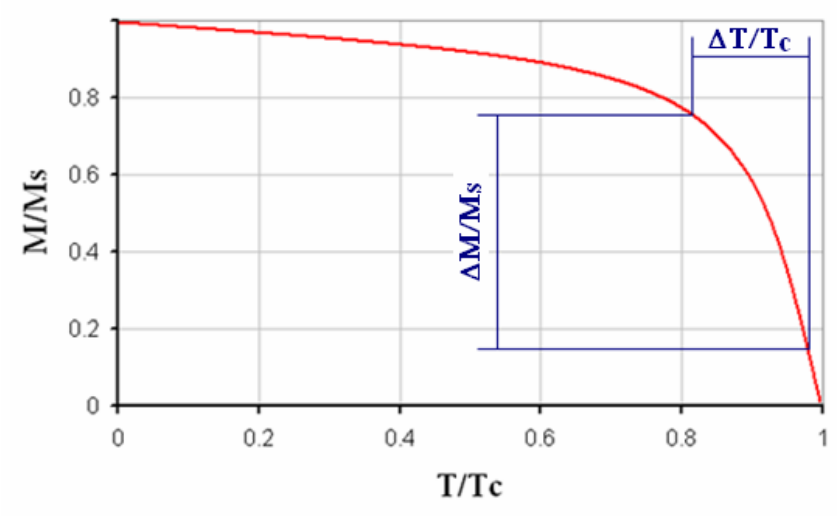

Figure 5.2 Representation of the magnetization dependence of temperature near the Curie temperature.

The maximum pressure increment that can be obtained from the magnetocaloric pump is reached when the ferrofluid reaches its curie temperature any additional heating would not increase the pumping capacity of the device. On the other hand if the maximum temperature reached by the ferrofluid is far from the Curie temperature the maximum change in magnetization would be small.

As mentioned in Chapter 3 the magnetization near the Curie temperature can be assumed as a linear function of the temperature (equation 3.2) and combining with equation 5.10; the pressure change experience by the ferrofluid inside the magnetocaloric pump can be expressed as:

$$\Delta p = \mu_0 HK\Delta T \qquad \textbf{5.11}$$

Equation 5.11 gives a prediction of pressure change experienced by a ferrofluid

with known pyromagnetic coefficient (K) and for a given temperature change.

5.2 Proposed Concepts

The prototype for the evaluation of the proposed concept is an open loop that allows to measure change in pressure by change in fluid height (see Figure 5.3). The ferrofluid flows from a reservoir into a vertical hose by the change in pressure produced by the magnetocaloric pump. In the prototype the heat input is controlled by changing the voltage applied to the heater in contact with the ferrofluid; temperatures are measured at the entrance and at the exit of the magnetocaloric pump.

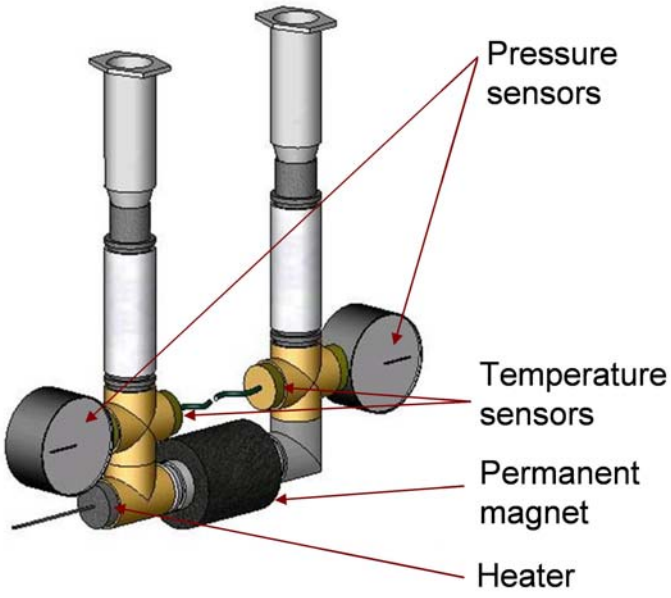

Figure 5.3 Representation of magnetocaloric pump prototype

The direction of the flow is guaranteed by the position of the heater. The fluid outside the magnetocaloric pump, which is in contact with the heater, will increase its

temperature and reduce its magnetization. The hot fluid will not try to displace the fluid inside the magnetocaloric pump as opposed to the other side of the pump where the fluid remains cold and displaces the hotter fluid. The direction of the flow is then determined by the position of the heater (see Figure 5.4).

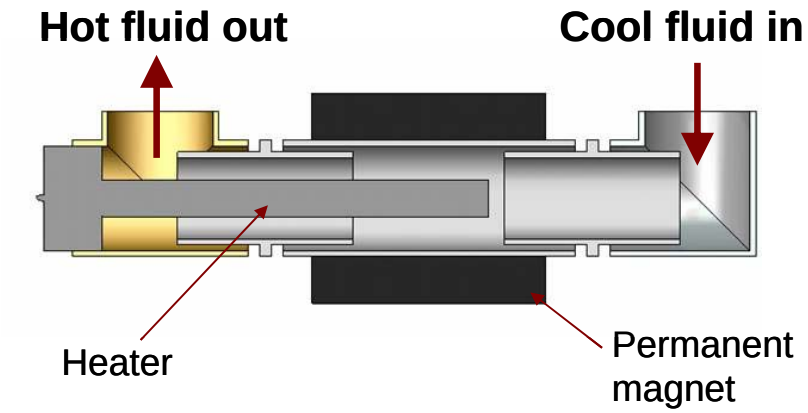

Figure 5.4 Schematic of the flow direction inside the magnetocaloric pump.

The prototype allows testing the device at different applied magnetic fields by interchanging the ring magnets; also the heater can also be interchange to obtained different heating region or different heating power. Figure 5.5 shows a picture of the actual prototype.

Figure 5.5 Magnetocaloric pump prototype during a test.

5.3 Preliminary Test

The preliminary tests of the magnetocaloric pump are carried out using permanent magnets with a magnetic induction of 0.15T. Two ferrofluids are compared: the first ferrofluid is a commercially available ferrofluid with magnetite nanoparticles suspended in water. The second ferrofluid contains $Mn_{0.7}Zn_{0.3}Fe_2O_4$ nanoparticles suspended in water. The properties of the two ferrofluids are presented in Table 5.1.

Nanoparticle	Base fluid	Density (kg/m^3)	Volumetric concentration (%)	Saturation magnetization (emu/g)
Magnetite (Fe_3O_4)	water	1260	3.5	12.96
MnZn ferrite ($Mn_{0.7}Zn_{0.3}Fe_2O_4$)	water	1055	2.5	4.91

Table 5.1 Properties of ferrofluids used in the magnetocaloric pump.

Results for both ferrofluids are presented in Figure 5.6. For this test the heater is placed coincident with the magnet at the entrance of the magnetocaloric pump section; the heater is set at maximum power to achieve the desired temperature difference and the pressure is measured as an increase in ferrofluid column height.

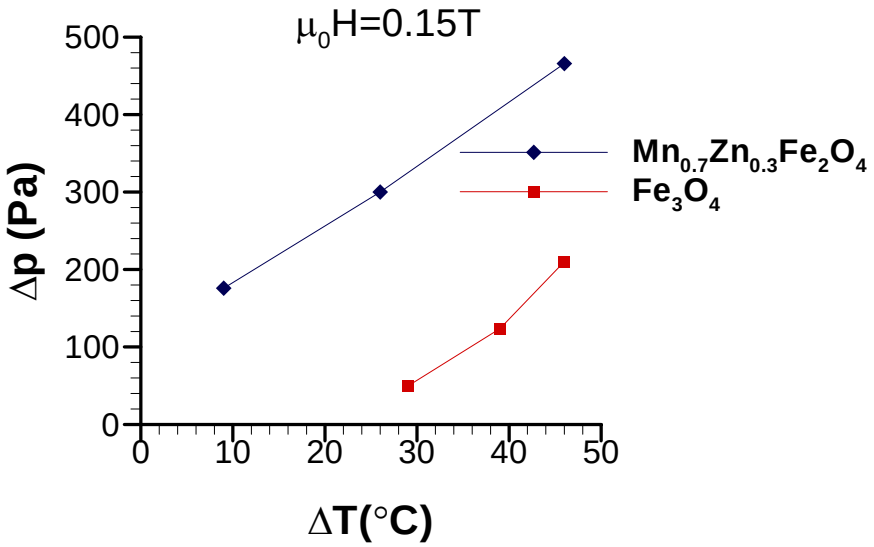

Figure 5.6 Pressure increment vs temperature change for ferrofluids composed of magnetite and MnZn ferrite nanoparticles.

From Figure 5.6 it is clear that the synthesized ferrofluid composed of MnZn ferrite nanoparticles works better with the magnetocaloric pump than the commercially available magnetite ferrofluid even at lower volumetric concentration. The MnZn ferrite ferrofluid experiences a pressure increase, inside the magnetocaloric pump, at temperature lowers than that of the magnetite ferrofluid even though the saturation magnetization is higher in the magnetite ferrofluid.

5.4 Research Issues

It was appreciated during the evaluation of the magnetocaloric pump that the concentration of the synthesized ferrofluid was decreasing and some of the nanoparticles were retain in the magnetic field. This behavior should be further analyzed to determine if the ferrrofluid has a maximum operational temperature below its boiling temperature where nanoparticles begin to settle out.

More detailed evaluation of the magnetocaloric pump is needed to determine practical parameters such as magnetic field length, heating length, optimal heating position with respect of magnetic field and optimal magnetization of the permanent magnet for a given application.

6 CONCLUSIONS AND FUTURE WORK

The concept of the magnetocaloric pump has been proved and implemented. Two different ferroflids were use in the evaluation of the magnetocaloric pump. Magnetic fluids with suspended Manganese-Zinc ferrite nanopaticles were synthesized and characterized and the following concluding remarks were reached:

Ferrofluids with $Mn_{0.7}Zn_{0.3}Fe_2O_4$ and $Mn_{0.8}Zn_{0.2}Fe_2O_4$ nanoparticles (x=0.7 and x=0.8) showed the best properties for the use in the magnetocaloric pump, having high saturation magnetization, high pyromagnetic coefficient and high initial susceptibility. The ferrofluid with $Mn_{0.5}Zn_{0.5}Fe_2O_4$ showed lower capabilities for the proposed application.

The most important property of the ferrofluid is a high pyromagnetic coefficient over the operational temperature range of the magnetocaloric pump and this characteristic does not imply that the Curie temperature has to be in the this temperature range.

The concentration of magnetic nanoparticles in the ferrofluid is a key aspect of the performance of the magnetic fluid, obtaining the best result at higher concentrations. At higher concentrations the viscosity is increased which is a negative aspect for the operation of the magnetocaloric pump but change in properties like saturation magnetization and pyromagnetic coefficient improve the performance of the device; this

suggest that magnetic properties are more important than rheological properties for this particular application.

Ferrofluids composed of MnZn ferrites show better behavior in the magnetocaloric pump applications for the proposed temperature range; this can be attributed to its higher pyromagnetic coefficient than that of the ferrofluid composed of magnetite.

Ferrofluid with higher concentration should be synthesized and tested in the magnetocaloric pump. Other types of base fluids should also be evaluated to find a ferrofluid with optimal properties and high stability. Obtain monodisperse ferrofluid with optimal particle size, to obtain maximum magnetization for a stable ferrofluid without a significant increment in viscosity. Complete the thermal characterization of the ferrofluid by measuring its specific heat. Finally it is recommended that a magnetocaloric pump prototype in a closed loop with refrigeration section should be constructed.

7 References

[1]. Lee, S., Choi, S.U.-S. Application of Metallic Nanoparticle Suspensions in advanced Cooling Systems, ASME Publications PVP-Vol. 342/MD-Vol. 72, 227-234, 1996.

[2]. Rosensweig, R. E., Ferrohydrodynamics, Dover, New York. 1997.

[3]. Resler, E. and Rosensweig, R. E. Regenerative thermomagnetic power. Journal of Energy and Power. 399-406, 1967.

[4]. Faghri, A, Heat pipe science and Technology, Taylor and Francis, Washington, DC. 1995.

[5]. Peterson, G.P., An Introduction to Heat Pipes: Modeling, Testing, and Applications, Wiley, New York. 1994.

[6]. Silverstein, C. Design and Technology of Heat Pipes for Cooling and Heat Exchange. Hemisphere Publishing Corporation, 1992.

[7]. http://www.dynatron-corp.com/products/heatpipe/heatpipe.asp?page=heatpipe

[8]. Love, L. J.; Jansen, J. F;Mcknight, T. E; Roh, Y. and Phelps, T. J. A magnetocaloric pump for microfluidic applications, IEEE transactions on nanobioscience, vol 3, n 2, 2004.

[9]. S. Shuchi, K. Sakatani and Hi. Yamaguchi An application of a binary mixture of magnetic fluid for heat transport devices. Journal of Magnetism and Magnetic Materials, In Press, Corrected Proof, Available online 15 December 2004.

[10]. H. Yamaguchi, A. Sumiji, S. Shuchi and T. Yonemura Characteristics of thermo-magnetic driven motor using magnetic fluid Journal of Magnetism and Magnetic Materials, Volumes 272-276, Part 3, May 2004.

[11]. Yamaguchi, H., Kobori, I. and Kobayashi, Characteristics of a magnetic fluid heat transport device-Part 1: numerical simulation of flow and heat transport phenomena, Proc Instn Mech Engrs, vol 214, 2000.

[12]. Ganguly, R., Sen, s. and Puri, I. K. heat transfer augmentation using a magnetic fluid under the influence of a line dipole. Journal of Magnetism and Magnetic Materials, 271, 63-73. 2004.

[13]. Auzans, E., Zins, D. Blums, E. and Massart, R. synthesis and properties of Mn-Zn ferrite ferrofluids. Journal of Materials Science. 34, 1253-1260. 1999.

[14]. Zins, D., Cabuil, V. and Massart, R. New aqueous magnetic fluids. Journal of

Molecular Liquids. 83, 217-232, 1999.

[15]. Bica, D., Vekas, L. and Rasa, M. Preparation and magnetic properties of concentrated magnetic fluids on alchohol and water carrier liquids. Journal of Magnetism and Magnetic Materials. 252, 10-12. 2002.

[16]. Hatton, T. A., Laibinisand P. E. and Shen. L. Aqueous magnetic fluids stabilized by surfactant bilayers. Journal of Magnetism and Magnetic Materials, Volume 194, Issues 1-3, 37-44. 1999.

[17]. Skumiel, A., Jozefczak, A., Hornowski, T. and Labowski, M. The influence of the concentration of ferroparticles in a ferrofluid on its magnetic and acoustic properties. Journal of Physiscs D: Applied Physiscs. 36, 3120-3124. 2003.

[18]. Maiorov, M., Blums, E., Hanson, M. and Johanson, C. high field magnetization of the colloidal Mn-Zn ferrite. Journal of Magnetism and Magnetic Materials, 201, 95-97. 1999.

[19]. Poddar, P., Srikanth, H., Morrison S.A., Carpenter, E. E. Inter-particle interactions and magnetism in manganese-zinc ferrite nanoparticles. Journal of Magnetism and Magnetic Materials, 288, 443-451. 2005.

[20]. Son, S., Swaminathan, R. and McHenry, M. E. Structure and magnetic properties of rf thermally plasma synthesized Mn and Mn–Zn ferrite nanoparticles. Journal of Applied Physics. 93. 2003.

[21]. Sattar, A. A., El-Sayed, H. M., El-Shokrofy, K. M. and El-tabey, M. M. Improvement of the magnetic properties of Mn-Ni-Zn ferrite by the non-magnetic $Al3^{+-}$ion substitution. Journal of Applied Science. 5, 162-168. 2005.

[22]. Amarendra, K. S., Goel, T. C. And Mendiratta, R. G. Effect of manganese impurity on the conductivity, dielectric behavior and magnetic properties of $Ni_{0.3}Mn_xZn_{0.7-x}Al_xFe_2O_4$. Japan journal of Applied Physics. 42, 2690-2691. 2003

[23]. Rezlescu, E., Sachelarie, L., Popa, P. D. And Rezlescu, N. Effect of substitution of divalent ions on the electrical and magnetic properties of Ni-Zn-Me ferrites. IEEE Transactions on Magnetism. 36, 3962-3967. 2000.

[24]. Breitzer, J. and Lisensky, G., Synthesis of aqueous ferrofluid, University of Wisconsin at Madison, Interdisciplinary group, MRSEC. 1999. http://mrsec.wisc.edu/edetc/nanolab/ffexp/index.html

[25]. Chinnasamy, C. N., Jeyadevan, B., Perales-Perez, O., Kasuya, A., Tohji, K. Growth dominant co-precipitation process to achieve high coercivity at room temperature in CoFe2O4 nanoparticles, Transactions IEEE Magnetics. 2002.

[26]. Perales O., Sasaki H., Jeyadevan B., Kasuya, A and Tohji, K. Production of monodispersed magnetic particles by using effective size selection methods at the

nanosize level. Journal of Applied Physics. 2002.

[27]. Xuan, Y. and Li, Q. Heat transfer enhancement of nanofluids. International Journal of Heat and Fluid Flow. 21, 58-64. 2000.

[28]. Caizer, C. Magnetic behaviour of $Mn_{0.6}Fe_{0.4}Fe_2O_4$ nanoparticles in ferrofluid at low temperatures. Journal of Magnetism and Magnetic Materials. 251, 304-315. 2002.

[29]. Yang, Y., Zhang, Z. G., Grulke, E. A., Anderson, w. B. and Wu, G. Heat transfer properties of nanoparticles-in-fluid dispersions (nanofluids) in laminar flow. International Journal of Heat and Mass Transfer. 48, 1107-1116. 2005.

[30]. Iusan, V., Buioca, C. D., Hadgia, S. Magnetic fluids of low viscosity. Journal of Magnetism and Magnetic Materials, 201, 38-40. 1999.

[31]. Wagh, D. K. and Avashia, A. On the viscosity of a magnetic fluid. Journal of Magnetism and Magnetic Materials, 153, 359-365. 1996.

[32]. Schmidt, A. M. Induction heating of novel thermoresponsive ferrofluids, Journal of Magnetism and Magnetic Materials. 2004.

[33]. Tangthieng, C., Finlayson, B. A., Maulbetsch, J., Cader, T., Heat transfer enhancement in ferrofluids subject to steady magnetic fields, Journal of Magnetism and Magnetic Materials. 201, 252-255. 1999.

[34]. Ivanov, A. and Mendelev, V. Magnetic properties of ferrofluids: an influence of chain aggregates Journal of Magnetism and Magnetic Materials, In Press, Corrected Proof, Available online 18 December 2004.

[35]. Ouakssim, A., Fastrez, S., Roch, A., Laurent, S., Gossuin, Y., Piérart, C., Vander Elst, L. and Muller, R. N. Control of the synthesis of magnetic fluids by relaxometry and magnetometry. Journal of Magnetism and Magnetic Materials. Volumes 272-276, Supplement 1. 2004.

[36]. Zabow, G., Assi, F., Jenks, R. and Prentiss, M. Guided microfluidics by electromagnetic capillary focusing. Applied Physics Letters, v 80, n 8. 2002.

[37]. Odenbach, S. Magnetic fluids-suspensions of magnetic dipoles and their magnetic control. Journal of Physics: condensed matter. 2003.

[38]. Tauxe, L. Paleomagnetic Principles and Practice. Springer. 2002

[39]. Wang, L., Fan, Z., Roy, A. G. and Laughlin, D. E. Effects of the atomic ordering on the Curie temperature of FePd $L1_0$ type alloys. Journal of Applied Physics, v 95, n 11. 2004.

[40]. Loudghiri, E., Nogues, M. Taibi, M. and Belayachi, A. Preparation and magnetic

interactions in Cd1-xZnxCr2Se4 spinel. Journal of Condensed Matter, v 5, n 1. 2004.

[41]. Liu, J. M., Yu, T., Huang, Q., Li, J., Shen, Z. X. and Ong, C. K. Magnetic polaron conduction above the Curie temperature in Fe-doped Pr0.75Sr0.25MnO3. Journal of Physics: Condensed Matter. 14, L141-L147. 2002.

[42]. Trainer, M. Ferroelectrics and the Curie-Weiss law. European Journal of Physiscs. 21, 459-464. 2000.

[43]. Papell S. S. Low viscosity magnetic fluid obtained by the colloidal suspension of magnetic particles US Patent Specification 3 215 572. 1964.

[44]. Odenbach S., Recent progress in magnetic fluid research, Journal of physics: condensed matter. 2004.

[45]. Odenbach, S., Magnetic fluids-suspensions of magnetic dipoles and their magnetic control, Journal of physics: condensed matter. 2003.

[46]. Schmidt, A. M. Induction heating of novel thermoresponsive ferrofluids, Journal of Magnetism and Magnetic Materials. 2004.

[47]. Blums, E. Heat and mass transfer phenomena, Journal of Magnetism and Magnetic Materials, Vol 252, 189-193. 2002.

[48]. Peralez-Perez, O., Calderón, E. and Melendez, C. Synthesis and characterization of Cobalt and Manganese-Zinc ferrites. Unpublished.

[49]. Gutierrez, G., Catano, J. E., Peralez-Perez, O., Tomar, M., Calderón, E. and Melendez, C. Characterization of Mn-Zn magnetic fluid for cooling applications at ambient temperature. Technical publication, ASME, Proceedings of IMECE November, 2005.

[50]. Vekas, L, Rasa, M. and Bica, D. Physical properties of magnetic fluids and nanoparticles from magnetic and magneto-rheological measurements. Journal of Colloid and Interface Science. 231, 247-254. 2000.

[51]. Xuan, Y. and Roetzel, W. Conceptions for heat transfer correlation of nanofluids International Journal of Heat and Mass Transfer, Vol 43, 3701-3707. 2000.

[52]. Kleinstreuer, C. and Koo, J. A new thermal conductivity model for nanofluids. Journal of nanoparticle research. 6, 577-588. 2004.

[53]. Choi, S. U. S. and Yu, W. The role of interfacial layers in the enhanced thermal conductivity of nanofluids: A renovated Maxwell model. Journal of nanoparticle research. 5, 167-171. 2003.

[54]. Choi, S. U. S., Zhang, Z. G., Yu W., lockwood, F. E. and Grulke, E. A.

Anomalous thermal conductivity enhancement in nanotube suspensions. Applied physics letters. 79, 14. 2001.

[55]. Prasher, R., Bhattacharya, P. and Phelan, P. E. Thermal conductivity of nanoscale colloidal solutions (nanofluids). Physical review letters. 94, 025901. 2005.

[56]. Grob, U., Song, Y. W. and Hahne, E. Measurements of liquid thermal conductivity and diffusivity by the transient hot-strip method. Fluid phase equilibria. 76, 273-282. 1992.

[57]. http://www.omega.com/temperature/Z/pdf/z033-035.pdf

[58]. Beckwith, T., Marangoni, R., and Lienhard, J., Mechanical Measurements, Addison_Wesley, Reading, MA. 1993

[59]. Kim, J. Abbay, S. Hoang, T. and Ku, J. Advanced Capillary Pumped Loop. Proceedings of 11th International Heat Pipe Conference, Japan, Sept. 1999.